Cell Reports

Article

MED13 and glycolysis are conserved modifiers of α-synuclein-associated neurodegeneration

Graphical abstract

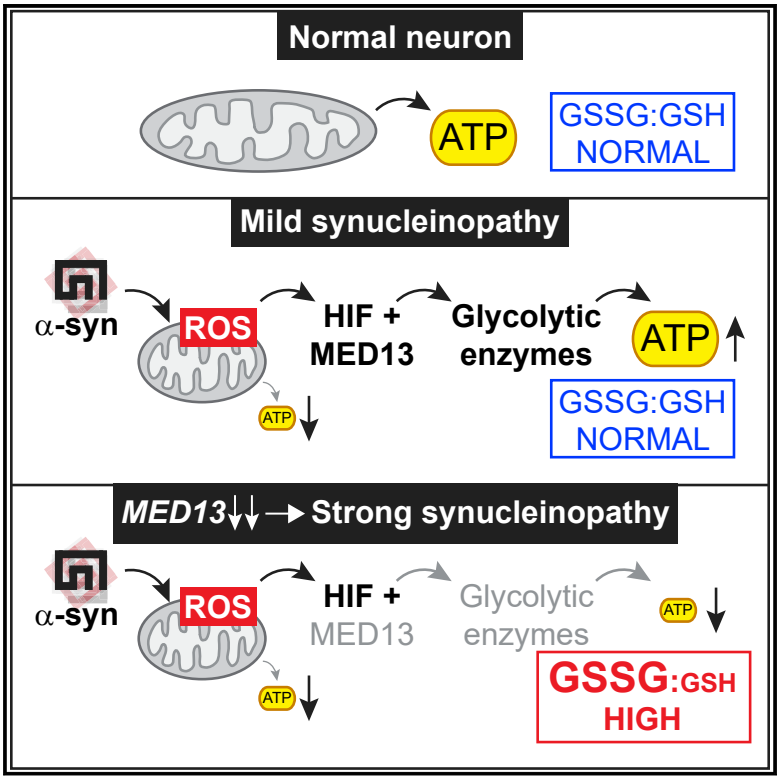

Highlights

- 12 conserved genes are identified as *SNCA* modifiers in flies
- Human ortholog of *skd*/*MED13* lies in Parkinson's GWAS locus
- In flies and mice, *SNCA* induces glycolytic enzymes through *MED13*
- Glycolysis protects against *SNCA*

Authors

Mengda Ren, Ying Yang, Kelsey Hwee Yee Heng, ..., Kah Leong Lim, Jing Zhang, Tong-Wey Koh

Correspondence

tongwey@tll.org.sg

In brief

Ren et al. identify 12 neuroprotective genes in a fly Parkinson's disease model. One gene, *MED13*, mediates induction of glycolytic enzymes by *SNCA* in flies and mice. Induction of glycolysis is protective against *SNCA*. Together, this work and previous GWAS data suggest that *MED13* is a Parkinson's disease risk gene.

Ren et al., 2022, Cell Reports *41*, 111852
December 20, 2022
https://doi.org/10.1016/j.celrep.2022.111852

CellPress

Cell Reports

CellPress
OPEN ACCESS

Article

MED13 and glycolysis are conserved modifiers of α-synuclein-associated neurodegeneration

Mengda Ren,[1,2,4,5,8] Ying Yang,[3,8] Kelsey Hwee Yee Heng,[1] Lu Yi Ng,[1] Claris Yuin-Yi Chong,[1] Yan Ting Ng,[1] Srinivas Gorur-Shandilya,[6] Rachel Min Qi Lee,[1,2] Kah Leong Lim,[4,5,9] Jing Zhang,[3,7,9] and Tong-Wey Koh[1,2,10,*]

[1]Temasek Life Sciences Laboratory, Singapore 117604, Singapore
[2]Department of Biological Sciences, National University of Singapore, Singapore 117558, Singapore
[3]Department of Pathology, Zhejiang University First Affiliated Hospital and School of Medicine, Hangzhou, Zhejiang 310002, China
[4]Lee Kong Chian School of Medicine, Nanyang Technological University, Singapore 308207, Singapore
[5]National Neuroscience Institute, Singapore 308433, Singapore
[6]Volen Center for Complex Systems, Brandeis University, Waltham, MA 02454-9110, USA
[7]China National Health and Disease Human Brain Tissue Resource Center, Hangzhou, Zhejiang 310002, China
[8]These authors contributed equally
[9]Senior author
[10]Lead contact
*Correspondence: tongwey@tll.org.sg
https://doi.org/10.1016/j.celrep.2022.111852

SUMMARY

α-Synuclein (α-syn) is important in synucleinopathies such as Parkinson's disease (PD). While genome-wide association studies (GWASs) of synucleinopathies have identified many risk loci, the underlying genes have not been shown for most loci. Using *Drosophila*, we screened 3,471 mutant chromosomes for genetic modifiers of α-synuclein and identified 12 genes. Eleven modifiers have human orthologs associated with diseases, including *MED13* and *CDC27*, which lie within PD GWAS loci. *Drosophila* Skd/Med13 and glycolytic enzymes are co-upregulated by α-syn-associated neurodegeneration. While elevated α-syn compromises mitochondrial function, co-expressing *skd/Med13* RNAi and α-syn synergistically increase the ratio of oxidized-to-reduced glutathione. The resulting neurodegeneration can be suppressed by overexpressing a glycolytic enzyme or treatment with deferoxamine, suggesting that compensatory glycolysis is neuroprotective. In addition, the functional relationship between α-synuclein, MED13, and glycolytic enzymes is conserved between flies and mice. We propose that hypoxia-inducible factor and MED13 are part of a druggable pathway for PD.

INTRODUCTION

Synuclein alpha (*SNCA*) encodes α-syn, a 140 amino acid protein, that is localized to various cellular compartments, including mitochondria and synapses.[1–3] α-Syn aggregates, such as oligomers and fibrils, have been associated with neuropathologies,[4–8] including Lewy bodies in Parkinson's disease (PD) and dementia with Lewy bodies (DLB).[9,10] In neurons of postmortem PD brains, α-syn aggregates correlate with lower mitochondrial volume density,[11] while in experimental models, pathogenic α-syn aggregates impair mitochondrial function.[12–14]

Understanding the genetics underlying synucleinopathies will help identify genetic risk predictors and drug targets. While below 5% of PD and DLB cases are familial and monogenic, the vast majority are sporadic and due to polygenic inheritance, environment, and aging.[15,16] Genome-wide association studies (GWASs) for PD and DLB show associations with numerous loci, including *SNCA*.[17,18] However, substantial proportions of genetic contribution remain unaccounted for. While rare variants may partially account for this missing heritability, genetic interactions between *SNCA* and other loci should be important.[19–21]

A powerful approach is to identify modifiers of a key disease risk factor, as previously executed for Huntington's disease.[22] Subsequent studies have successfully identified modifiers of synucleinopathies associated with *LRRK2* and *GBA* pathogenic mutations.[23–25] Due to conservation of pathways, efforts in genetic model organisms have complemented human genetics in revealing genetic interactions relevant to human synucleinopathies.[14,26–39]

To identify dominant genetic modifiers, expression of transgenic *SNCA* in *Drosophila* neurons was combined with heterozygous mutations randomly generated by chemical mutagenesis. Successive rounds of locomotor and brain morphological assays identified 12 *SNCA*-modifier genes. Two have human orthologs, *MED13* and *CDC27*, that are associated with PD GWAS risk loci. Further characterization of *MED13* in fly and mouse models of synucleinopathy indicates a role in inducing compensatory glycolysis which protects against neurodegeneration.

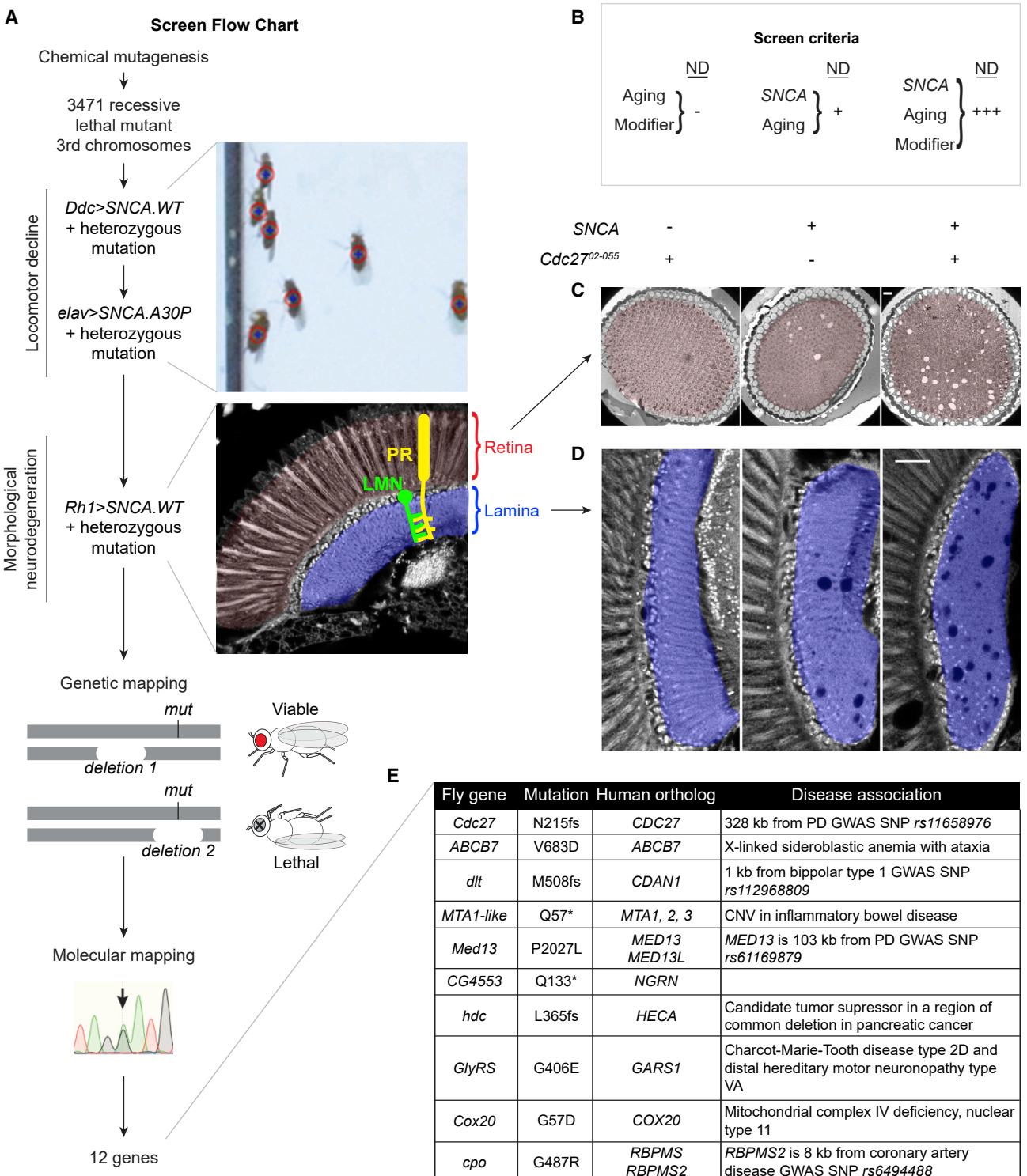

Fly gene	Mutation	Human ortholog	Disease association
Cdc27	N215fs	*CDC27*	328 kb from PD GWAS SNP *rs11658976*
ABCB7	V683D	*ABCB7*	X-linked sideroblastic anemia with ataxia
dlt	M508fs	*CDAN1*	1 kb from bippolar type 1 GWAS SNP *rs112968809*
MTA1-like	Q57*	*MTA1, 2, 3*	CNV in inflammatory bowel disease
Med13	P2027L	*MED13 MED13L*	*MED13* is 103 kb from PD GWAS SNP *rs61169879*
CG4553	Q133*	*NGRN*	
hdc	L365fs	*HECA*	Candidate tumor supressor in a region of common deletion in pancreatic cancer
GlyRS	G406E	*GARS1*	Charcot-Marie-Tooth disease type 2D and distal hereditary motor neuronopathy type VA
Cox20	G57D	*COX20*	Mitochondrial complex IV deficiency, nuclear type 11
cpo	G487R	*RBPMS RBPMS2*	*RBPMS2* is 8 kb from coronary artery disease GWAS SNP *rs6494488*
ND-39	W319*	*NDUFA9*	Mitochondrial complex I deficiency, nuclear type 26
Eip75b	R750*	*NR1D1 NR1D2*	*NR1D1* intron contains multiple sclerosis GWAS SNP *rs883871*

(legend on next page)

RESULTS

A *Drosophila* screen identified 12 dose-sensitive modifiers of *SNCA*-associated neurodegeneration

We hypothesized that some genetic modifiers interact with *SNCA* to enhance neurodegeneration but only cause neurodegeneration in the presence of disease-associated SNPs near *SNCA*. These hypothetical modifier alleles are likely to persist as relatively common variants in heterozygous states and may not lead to disease. We further posited that many modifier alleles affect highly conserved biological processes due to the conserved nature of neuronal function.[40] To test this, we performed a screen for dose-sensitive genes that modify *SNCA*-associated neurodegeneration in *Drosophila*. We generated 3,471 recessive lethal strains with mutant third chromosomes using ethyl methanesulfonate (EMS) chemical mutagenesis. Then, we screened heterozygous mutant flies using age-dependent locomotor decline and brain morphology (Figure 1A). To identify the type of modifiers hypothesized above, we adopted a strict set of criteria (Figure 1B): (1) a heterozygous modifier alone does not cause neurodegeneration, and (2) it will only enhance or suppress neurodegeneration associated with *SNCA* expression.

We screened for locomotor decline in two successive iterations by combining *SNCA*-expressing transgenes with heterozygous mutant chromosomes (Figures 1A and S1A; STAR Methods), retaining 281 and 41 mutant strains, respectively. To test for morphological modification of *SNCA*-associated neurodegeneration, we combined these 41 mutant strains with *Rh1-GAL4* and *UAS-SNCA.WT*. This pair of transgene expresses wild-type *SNCA* specifically in photoreceptor (PR) neurons R1–R6, which project axons from the retina to form en passant synapses with lamina monopolar neurons (LMNs) in the lamina (Figure 1A). Degenerating PR neurons manifest as "holes" or vacuoles in the retina and lamina (Figures 1A, 1C, and 1D). *SNCA* expression using the *Rh1-GAL4* driver did not cause eye developmental defects and exhibited age-dependent neurodegeneration (Figures S1C, inset, and S1C′). This morphological screen identified 12 mutants that enhance *SNCA*-associated neurodegeneration (Figures S1B and S1C).

Genetic mapping and sequencing allowed us to identify 12 candidate modifier genes (Figures 1A, 1E, and S1D; Tables S1 and S2; STAR Methods). For example, to map the modifier allele *06-056*, we determined its approximate position using meiotic recombination with previously described genetic markers located across the third chromosome (see genetic markers and recombinational distances in Figure S2A).[41] Using molecularly defined chromosomal deletions,[42] complementation tests identified a ~190 kb region containing 19 candidate genes. Using genetic and molecular methods (Figure S2A; Table S2), we identified the mutation in a previously characterized gene, *skuld (skd)/Med13*.[43] We thus renamed the modifier allele as *skd/Med*$^{06-056}$. Additionally, genetic rescues and phenocopy experiments verified that each of the 12 modifier genes was responsible for the enhancement of *SNCA*-associated morphological neurodegeneration (Table S1; Figure S1C; STAR Methods). The 12 modifier genes have one or more human orthologs, and 11 are associated with human diseases (Figure 1E; Table S1).[17,44–54]

To test whether the *SNCA* enhancers increased the total level of α-syn or its phosphorylation at serine position 129 (pS129), we examined sodium dodecyl sulfate (SDS)-solubilized lysates in flies expressing *SNCA* with heterozygous modifier mutant chromosome. Here, we replicated previous data showing that α-syn undergoes phosphorylation at S129 in *Drosophila* neurons.[55] Interestingly, none of the modifiers affected the levels of total α-syn or pS129 (Figure S1E). Therefore, all 12 modifiers are likely to modify *SNCA*-associated neurodegeneration without directly altering α-syn at the protein level.

Drosophila skd/Med13 acts cell autonomously to protect neurons against *SNCA*-associated neurodegeneration

Here, we will focus on *skd/Med13* because its human ortholog is close to a PD GWAS variant[17] and expression quantitative trait locus (eQTL) analyses[56–60] suggest a correlation between *Med13* expression and the PD phenotype (Figures S2B and S2C). The evolutionarily conserved Mediator complex bridges transcription factors with the core transcriptional machinery.[61] Skd/Med13 is a subunit of the kinase module of the Mediator complex; this kinase module acts as a dissociable switch in regulating transcription at some genes where the core Mediator complex resides.[62,63] The *SNCA* modifier allele, *skd/Med13*$^{06-056}$, is predicted to result in a proline-to-leucine amino acid substitution at a conserved residue in the MID MedPiwi core

Figure 1. A *Drosophila* screen identified 12 dominant modifiers of *SNCA*

(A) Flow chart depicts the genetic screen involving locomotor and morphology assays, followed by genetic and molecular mapping (see STAR Methods). Morphological neurodegeneration of flies expressing *SNCA* in photoreceptor (PR) neurons R1–R6 (shown in yellow) were analyzed with respect to retina (shaded red) and lamina (shaded blue). In the lamina, lamina monopolar neurons (LMNs; shown in green) form extensive synapses with PR neurons R1–R6. Genetic mapping was performed by complementation tests between the screen mutants and previously characterized lethal alleles of known genes as well as deficiency strains. Complementation data was further confirmed with genetic rescues using wild-type copy of genomic fragments containing the candidate genes (Table S2). Molecular lesions were identified using a combination of Sanger sequencing and massively parallel genome sequencing. Genotypes were as follows: *Ddc-GAL4/+*; *mut/UAS-SNCA.WT* (first locomotor screen), *elav-GAL4/+*; *mut/UAS-SNCA.A30P* (second locomotor screen) and *Rh1-GAL4/+*; *mut/UAS-SNCA.WT* (morphological screen).

(B) Screen criteria for *SNCA* modifiers. "ND" indicates the extent of neurodegeneration. Left, middle and right columns correspond to panels in (C) and (D) directly below.

(C and D) Retina (C) and lamina (D) sections of three genotypes, *Rh1-GAL4/+*; *Cdc27*$^{02-055}$*/+*, *Rh1-GAL4/+*; *UAS-SNCA/+*, and *Rh1-GAL4/+*; *Cdc27*$^{02-055}$*/UAS-SNCA.WT*. Scale bars indicate 20 μm.

(E) All 12 *Drosophila SNCA* modifiers have human orthologs, of which 11 are associated with human diseases. The second column indicates predicted changes to the amino acid sequences in our mutants.

See also Figure S1 and Table S1.

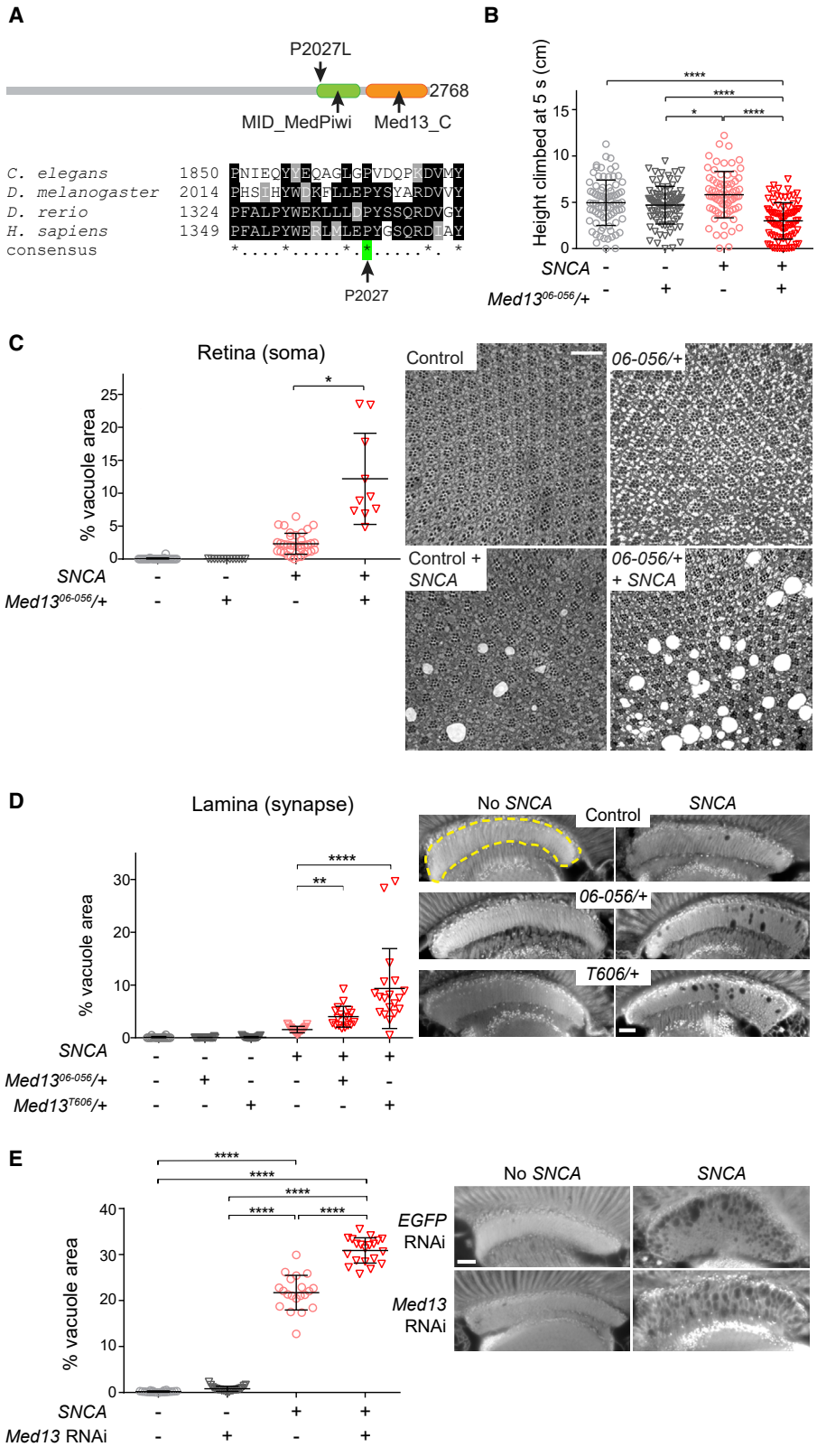

(legend on next page)

globular domain of Med13 (Figure 2A).[64] Heterozygous *skd/Med13*$^{06\text{-}056}$ only exhibited significant locomotor decline when combined with pan-neuronal *SNCA* expression, suggesting a synergistic interaction between *SNCA* expression and *skd/Med13* (Figure 2B).

To investigate the *SNCA-skd/Med13* interaction, we used *Rh1-GAL4* to drive *SNCA.WT* expression in PR neurons and examined morphological neurodegeneration (Figure 1A). *SNCA* expression alone led to a small number of vacuoles in neuronal cell bodies and synapses in 14-day-old flies (Figures 2C and 2D). Transmission electron microscopy suggests that the vacuoles reside within PR neurons (Figure S2D). Combining *SNCA* expression and heterozygous *skd/Med13*$^{06\text{-}056}$ mutation led to a significant increase in the fractional area occupied by vacuoles in both retina and lamina, while *skd/Med13*$^{06\text{-}056}$ heterozygotes did not show any vacuolization. Likewise, two additional alleles, *skd/Med13*^{T606} and *skd/Med13*^{MI12229}, also enhanced *SNCA*-associated neurodegeneration (Figures 2D and S1C). Similarly, *skd/Med13* knockdown led to a significant increase in neurodegeneration compared with *SNCA* expression alone; *skd/Med13* knockdown alone did not cause any degeneration (Figures 2E and S2E). Therefore, *skd/Med13* acts cell autonomously to protect neurons from *SNCA*-associated neurodegeneration.

Since Med13, Med12, cyclin C, and Cdk8 together form the evolutionarily conserved kinase module of the Mediator complex,[61] we asked whether knocking down the fly homologs encoding these subunits will enhance *SNCA*-associated neurodegeneration. Indeed, knockdown enhanced neurodegeneration in PR neurons expressing *SNCA* (Figure S2F).

In summary, a mild dose reduction of *skd/Med13* in neurons is sufficient to worsen neurodegeneration induced by *SNCA*. This conclusion is bolstered by data showing that all members of the Mediator kinase module are required to protect against *SNCA*-associated neurodegeneration.

SNCA induces expression of Med13 and glycolytic enzymes in fly brains

To further understand the role of *skd/Med13* in neuroprotection, we examined its expression in response to *SNCA.WT* expression. In larval brains expressing *SNCA*, *skd/Med13* mRNA and its corresponding protein are upregulated compared with brains not expressing *SNCA* (Figures 3A and S3A). Hence, *skd/Med13* upregulation appears to be an early response to neuronal stress associated with *SNCA* expression.

The kinase module is required for inducing glycolysis in mammalian cells.[65] To determine whether upregulation of Skd/Med13 protein is correlated with an increase of enzymes involved in glucose metabolism in larval brains (Figure 3B), we examined levels of enzymes thought to be rate limiting, suppress neurodegeneration, or extend lifespan.[27,66–69] *Lactate dehydrogenase* (*Ldh*) levels showed significant upregulation in *SNCA*-expressing brains compared with controls, whereas *phosphoglucose isomerase* (*Pgi*), *phosphofructose kinase* (*Pfk*), *phosphoglycerate kinase* (*Pgk*), *triosephosphate isomerase* (*Tpi*), and *glucose-6-phosphate dehydrogenase* (*G6pd*) showed small increases that were not statistically significant (Figure 3C). However, Pgi and Ldh proteins showed significant upregulation in *SNCA*-expressing brains compared with controls (Figure 3D).

In adult brains expressing *SNCA*, Pgi and Ldh were progressively upregulated with age (Figure 3E); Ldh upregulation is accompanied by a significant increase in neuronal lactate as detected by the genetically encoded fluorescence resonance energy transfer (FRET) sensor, Laconic (Figure 3F).[70] Similarly, we observed a strong increase of *hexokinase-A* (*Hex-A*) transcripts and a weak increase of *Hex-C* transcripts in *SNCA*-expressing brains (Figure S3B). In contrast, *G6pd* and *phosphogluconate dehydrogenase* (*Pgd*) transcripts, which code for NADPH-generating enzymes in the pentose phosphate pathway, were downregulated in *SNCA*-expressing brains. In addition, components of the α-ketoglutarate dehydrogenase complex in the Krebs cycle were not significantly altered by *SNCA* expression (Figure S3C). Hence, *SNCA* expression is associated with an upregulation of some glycolytic enzymes.

We considered the alternative possibility that Skd/Med13 may inhibit cell cycle re-entry for neuroprotection since the kinase module mediates expression of the cell-cycle inhibitor *p21*^{WAF1} in cancer cell lines.[71] After day 5 of adulthood, normal fly brains do not contain proliferating cells[72]; hence, proliferation marker expression could suggest cell cycle re-entry. Using antibodies (Figure S3D), expression of cell-cycle markers phospho-histone H3 (PH3) and proliferating cell nuclear antigen (PCNA) was not observed in adult PRs expressing *SNCA* (Figure S3E).

Skd/Med13 knockdown enhances oxidative stress caused by α-syn in fly neurons

Since elevated α-syn levels are known to impair mitochondrial function and induce oxidative stress,[14,73] we examined mitochondrial morphology in PR synapses of 14-day-old flies expressing combinations of *SNCA.WT* and *skd/Med13* RNAi. While

Figure 2. *Med13* is a dominant modifier of *SNCA*

(A) The *SNCA* modifier allele *Med13*$^{06\text{-}056}$ encodes a proline-to-leucine substitution at a conserved position in the core globular domain (PFam: PF18296).

(B) Heterozygous *Med13*$^{06\text{-}056}$ enhanced locomotor decline associated with pan-neuronally expressed *SNCA.A30P* 3-week-old flies.

(C) Heterozygous *Med13*$^{06\text{-}056}$ enhanced *SNCA*-associated degeneration at the PR soma layer in the retina in 2-week-old flies. Images on the right show Spurr's resin-embedded retina sectioned at ~90° to the PR neurons.

(D) Heterozygous *Med13*$^{06\text{-}056}$ and *Med13*^{T606} enhanced *SNCA*-associated degeneration at PR axon terminals in paraffin-embedded lamina in 2-week-old flies. Yellow dotted lines indicate the lamina region. See also Figure S1C for the enhancement of *SNCA*-associated degeneration in lamina by *Med13*^{MI12229}.

(E) PR-specific expression of *Med13* RNAi HMS01305 enhanced *SNCA*-associated degeneration at PR axon terminals in paraffin-embedded lamina in 2-week-old flies.

SNCA in (C)–(E) were expressed specifically in PR neurons R1–R6 using *Rh1-GAL4*. Data are plotted as means with standard deviations (SDs). Each point represents data from one fly ($n \geq 70$, 10, 17, and 20 for B, C, D, and E, respectively). Analyzed with Kruskal-Wallis test followed by Dunn's multiple comparisons test. *$p < 0.05$, **$p < 0.01$, and ****$p < 0.0001$. Scale bars represent the following dimensions: 100 μm in (C) and 20 μm in (D) and (E).

See also Figure S2.

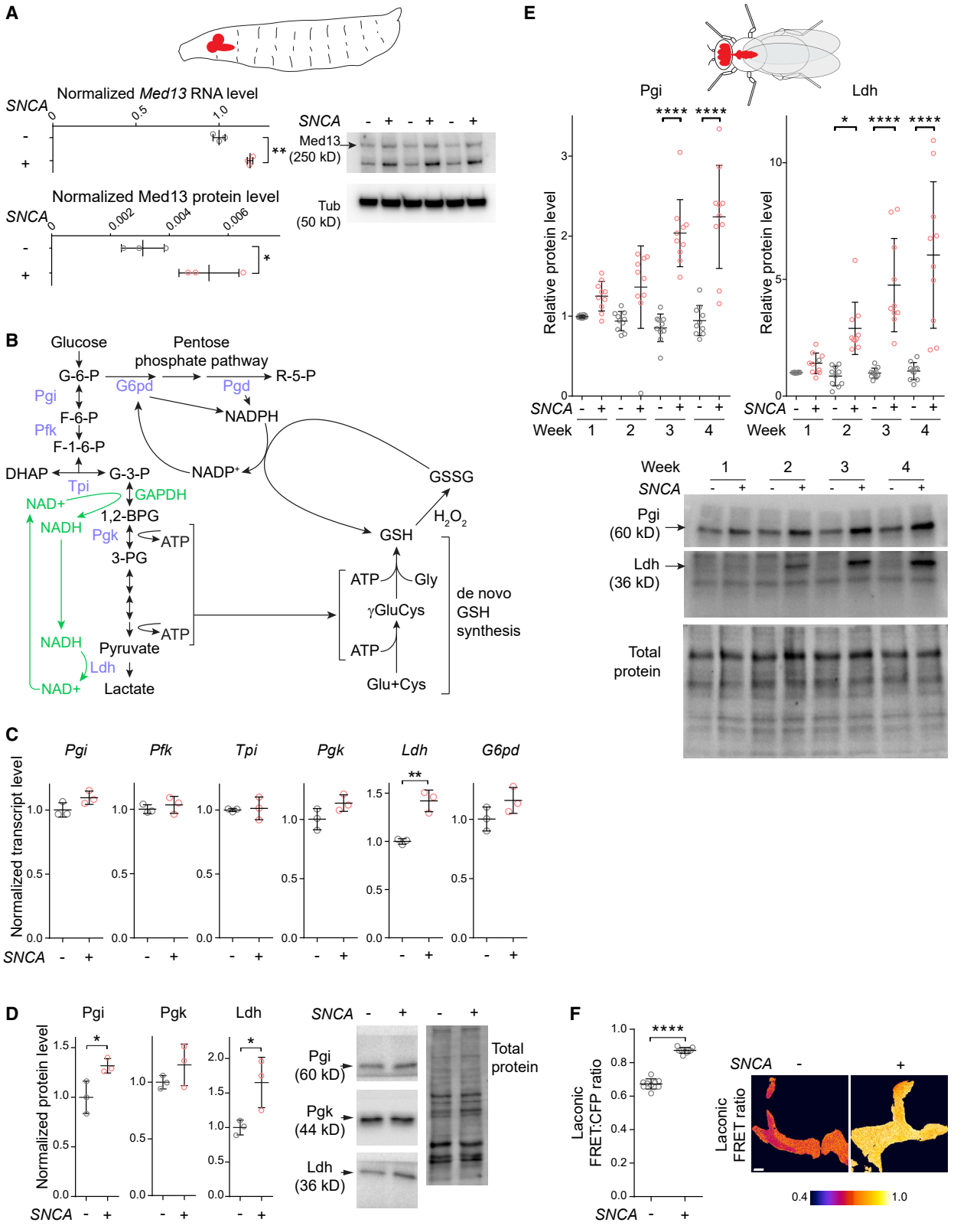

(legend on next page)

mitochondria in synapses without *SNCA* expression have elongated morphology, those expressing *SNCA* were less elongated and more rounded as measured by lower prolate ellipticity (Figure 4A). Synapses expressing *SNCA* also showed a significant increase in the fraction of mitochondria in the smallest size range of less than 0.1 μm^3 and a significant decrease of the fraction in the largest size range of more than 1 μm^3 (Figures 4B, S4A, and S4B). *skd/Med13* knockdown significantly increased overall mitochondrial volume without altering the fraction of mitochondria in the <0.1 μm^3 range. Comparing synapses co-expressing *SNCA* and *skd/Med13* RNAi with those expressing only *SNCA*, fractions of small mitochondria (<0.1 μm^3) were similar, while fractions of large mitochondria (>1 μm^3) were slightly increased but was not statistically significant. This indicates that *SNCA* overexpression leads to accumulation of a subset of shorter and smaller mitochondria, consistent with previous work,[13] while *skd/Med13* knockdown may cause a slight increase in the fraction of the larger mitochondria.

As mitochondria fragmentation has been associated with oxidative stress, we expressed a mitochondria-targeted sensor for H_2O_2, mito-roGFP2-Orp1,[74] in PR neurons using *Rh1-GAL4*. In 7-day-old flies, PR synapses did not show strong differences regardless of *SNCA* and/or *skd/Med13* expression (Figures 4C and S4C). However, 14-day-old flies expressing *SNCA* (with and without *skd/Med13* RNAi) showed higher mitochondrial H_2O_2 than those not expressing *SNCA*. This suggests that *SNCA* expression leads to mitochondrial oxidative stress regardless of *skd/Med13* status.

Since mitochondrial oxidative phosphorylation and glycolysis are both sources of ATP, compromised mitochondria and induction of glycolysis may influence ATP levels. Therefore, we examined relative ATP levels by expressing a genetically encoded FRET sensor of ATP in PR neurons.[75] Compared with controls expressing *EGFP* RNAi, synapses expressing *skd/Med13* RNAi or *SNCA* led to small perturbations of ATP levels that were not statistically significant (Figure 4D); however, ATP levels were significantly lower in synapses co-expressing *skd/Med13* RNAi and *SNCA*. To further examine ATP levels, we adapted an *in vivo* luciferase assay by expressing the ATP-dependent firefly luciferase in all neurons.[76,77] Compared with control flies without RNAi and *SNCA* expression, *skd/Med13* knockdown significantly reduced luciferase bioluminescence in 10- and 13-day-old flies (Figure S4D). Flies expressing *SNCA* showed a decrease in bioluminescence, which was only significant at day 13, while a combination of *SNCA* expression and *skd/Med13* knockdown showed a strong decrease at both time points. Taken together, *skd/Med13* knockdown in the presence of *SNCA* expression led to a significant reduction of neuronal ATP.

Glutathione (GSH) synthesis involves two ATP-dependent steps, and millimolar concentrations of GSH are generated in neural cells as a major scavenger for H_2O_2 (Figure 3B).[78,79] Hence, we predicted that a combination of increased H_2O_2 and reduced ATP would perturb redox homeostasis. To determine whether *skd/Med13* knockdown enhanced oxidative stress associated with *SNCA* expression, we used a genetically encoded biosensor, cyto-Grx1-roGFP2, to estimate the GSH disulfide-to-GSH ratio (GSSG:GSH) in neuronal cytoplasm.[74] Seven-day-old flies only showed small differences in GSSG:GSH ratio between genotypes (Figures 4E and S4E). However, 14-day-old flies co-expressing *skd/Med13* RNAi and *SNCA* showed significantly higher GSSG:GSH ratios than all other genotypes, suggesting a strong increase in oxidative stress in neurons. Taken together, combining *SNCA* expression and *skd/Med13* knockdown decreased ATP levels and increased oxidative stress in neurons.

Overexpressing *Pgi* and *Pfk* counteracts *SNCA*-associated neurodegeneration that is enhanced by *skd/Med13* knockdown in fly neurons

As Skd/Med13 was co-upregulated with glycolytic enzymes in response to *SNCA* expression in fly brains, we examined whether *skd/Med13* knockdown would affect glycolytic enzyme levels. We used RNAi-validated antibodies to stain for Pgi, Pgk, and Ldh in the fly retina (Figure S5A). Protein levels were unchanged when *skd/Med13* function was reduced in the absence of *SNCA* expression (Figures 5A and S5B). Interestingly, reducing *skd/Med13* function in the presence of *SNCA* expression significantly reduced enzyme levels. To determine if the relationship between *SNCA*, *skd/Med13*, and glycolytic enzymes is generalizable to all neurons, a pan-neuronal driver was used. Compared with brains expressing only *SNCA* (Figure 5B), brains co-expressing *skd/Med13* RNAi and *SNCA* showed a significant reduction of Ldh, while Pgi showed a slight decrease, which was not statistically significant. Hence, *skd/Med13* is required in neurons for the induction of a subset of glycolytic enzymes by *SNCA* expression.

Figure 3. *SNCA* expression in fly neurons upregulates Med13 and glycolytic enzymes

(A) Brains from *nSyb-QF2 QUAS-SNCA*/+ larvae were compared with *nSyb-QF2*/+ controls for *Med13* transcripts (top left) and Med13 protein levels (right and bottom left). Med13 protein levels were normalized to total protein levels (see Figure S3A).

(B) Diagram showing glycolysis, pentose phosphate pathway, and glutathione homeostasis. Enzymes tested for expression levels are indicated in purple. NAD+ regenerated by Ldh is utilized by GAPDH, a process that drives glycolysis when NAD+ is limited (green).

(C) Transcript levels of enzymes in glycolysis and pentose phosphate pathway in larval brains with and without *SNCA* expression.

(D) Protein levels of Pgi, Pgk, and Ldh with and without *SNCA* expression.

(E) Brains from *nSyb-QF2 QUAS-SNCA*/+ adults were compared with *nSyb-QF2*/+ controls for Pgi and Ldh protein levels at weeks 1–4 of adult stage.

(F) Neuronal lactate levels in brains from 3-week-old *nSyb-QF2 QUAS-SNCA*/+ adults were compared with *nSyb-QF2*/+ controls using fluorescence resonance energy transfer (FRET) of a lactate biosensor, Laconic, which was expressed specifically in neurons.

Levels of each transcript were calculated using *ed* and *rpl32* as internal controls (see STAR Methods), both of which are not affected by *SNCA* expression. Protein levels were normalized to total protein levels. Transcripts and protein levels are normalized to "no *SNCA*" controls. Data are plotted as means with SDs. Each point represents data from one biological replicate (n = 3 for A, C, and D, 10 for E, and $\geq$8 for F). Analyzed with t test (A–D), and one-way ANOVA followed by Tukey's multiple comparisons test (E). *$p < 0.05$, **$p < 0.01$, and ****$p < 0.0001$. Scale bar represents 20 μm in (F).

See also Figure S3.

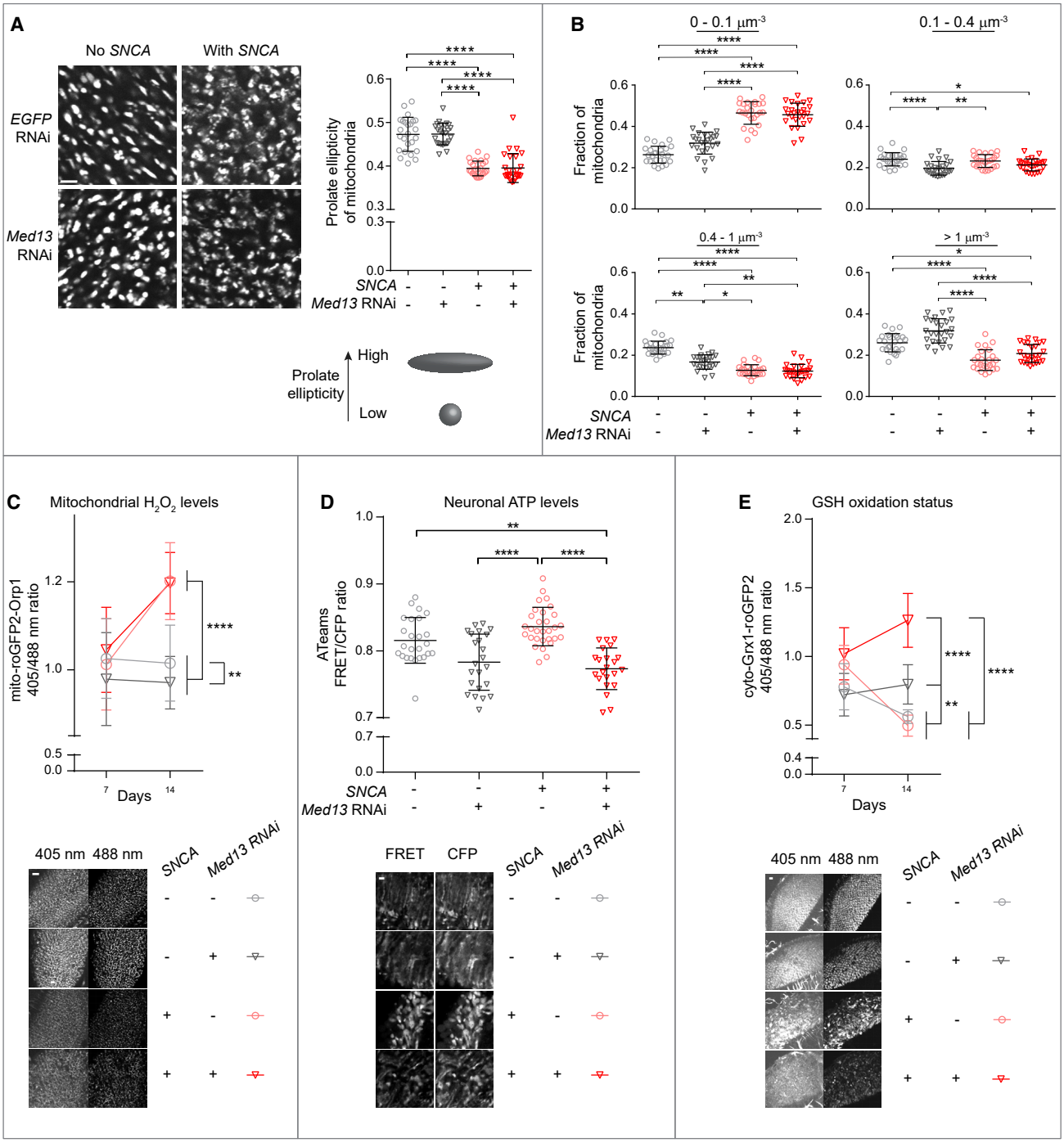

Figure 4. *SNCA*-associated mitochondrial impairment combined with *Med13* knockdown decreased ATP and increased oxidative stress

(A–C) *Rh1-GAL4* was used to express mito-roGFP2-Orp1 in PR synapses for measurements of mitochondrial morphology and relative mitochondrial H_2O_2 levels.

(A) Mitochondria labeled with mito-roGFP2-Orp1 shows that *SNCA* expression is associated with changes from high prolate ellipticity (cigar-like morphology) to low prolate morphology (spherical morphology).

(B) Mean volumes of mitochondria from individual flies of the experiment in (A) were separated into large size categories of 0–0.1, 0.1–0.4, 0.4–1.0, and >1 μm^3 to compare the distribution of mitochondria of each size category across the genotypes.

(C) Relative mitochondrial H_2O_2 levels were measured using mito-roGFP2-Orp1 as 405:488 nm fluorescence ratios, where an increased ratio indicates higher levels.

(D) Relative ATP levels were measured using the AT1.03NL FRET sensor expressed in PR neurons using *Rh1-GAL4* in 14-day-old flies. Higher YFP/CFP ratios indicate higher ATP levels.

(legend continued on next page)

To determine if induction of Pgi and G6pd is neuroprotective, we co-expressed them with *skd/Med13* RNAi and *SNCA* in PR neurons. *Pgi* overexpression produced a strong suppression of neurodegeneration to levels less than flies expressing only *SNCA* (Figures 5C and S5C), while *G6pd* overexpression suppressed neurodegeneration to a level similar to that of *SNCA* expression alone. Hence, this suggests that artificially upregulating glycolysis and pentose phosphate pathways are likely to be protective against *SNCA*-associated neurodegeneration.

Prompted by the strong rescue of neurodegeneration by *Pgi*, we asked if *Pgi* affects levels of total α-syn protein and its pS129 status. *Pgi* knockdown in *SNCA*-expressing neurons was associated with slight, but not significant, increases of total α-syn and pS129 (Figure S5D).

As co-expression of *skd/Med13* RNAi and *SNCA* synergistically increased GSH oxidation levels (Figure 4E), we asked if *Pgi* overexpression affects GSH in this genotype. Indeed, co-overexpression of *Pgi* with *skd/Med13* RNAi and *SNCA* suppressed GSSG:GSH ratios to that of controls without *SNCA* or *skd/Med13* RNAi expression (Figure 5D).

As Pgi catalyzes its reaction in a bidirectional manner (Figure 3B),[80] Pgi overexpression may have increased the flux through the pentose phosphate pathway instead of glycolysis in our model. Since Pfk drives glycolysis in a unidirectional manner, we tested co-expression of *Pfk* with *skd/Med13* RNAi and *SNCA* (Figure S5E); here, *Pfk* overexpression significantly suppressed neurodegeneration. In addition, we co-expressed *Ldh* with *SNCA*; in this case, *Ldh* overexpression caused a slight, but significant, worsening of neurodegeneration (Figure S5F).

Taken together, the data in Figures 3 and 5 indicate that Skd/Med13 induction in response to *SNCA* expression is important to upregulate a subset of glycolytic enzymes. Interestingly, neuronal overexpression of *Pgi* and *Pfk*, but not *Ldh*, partially counteracted *SNCA*-associated neurodegeneration. Importantly, our analysis of GSH oxidation status suggests that *Pgi* overexpression counteracts the combined effect of *skd/Med13* RNAi and *SNCA* expression by restoring GSSG:GSH ratios to normal levels.

Drosophila hypoxia-inducible factor (Sima/Hif) acts cell autonomously to protect neurons, probably in a *Med13*-dependent manner

As the mammalian Mediator kinase module functions together with HIF1A to induce glycolytic enzymes,[62] we examined whether the fly homolog Sima/Hif is induced in response to *SNCA* expression. In fly larval brain extracts, we observed that *SNCA* expression was associated with a weak, but non-significant, increase in Sima/Hif protein and a significant increase in *sima/Hif* transcript (Figures S5G and S5H). The upregulation of Sima/Hif protein in larval brains only occurred in sporadic neurons (Figure S5J), which may explain the lack of strong upregulation in western blot.

We then asked if the Sima/Hif pathway is neuroprotective in *SNCA*-expressing fly neurons using validated RNAi transgenes (Figures S5K, 5E, and 5F). *sima/Hif* knockdown led to a highly significant increase in neurodegeneration in *SNCA*-expressing neurons. Conversely, knocking down either negative regulator of *sima/Hif*, *Hif prolyl hydroxylase* (*Hph*) and *von Hippel-Lindau* (*Vhl*), suppressed *SNCA*-associated neurodegeneration. Hence, this indicates that the Sima/Hif pathway is protective against α-syn in fly neurons.

We further tested whether pharmacologically activated neuroprotection by Sima/Hif depends on *Med13* function. Under normal conditions, Sima/Hif is continuously degraded through sequential modifications by Hph and Vhl (Figure 5E).[81] Deferoxamine (DFO) is known to inhibit Hph by sequestering its iron cofactor.[82] DFO induced the accumulation of Sima/Hif protein in fly brains in a dose-dependent manner (Figure S5I). We then asked whether DFO can protect against the accelerated loss of dopaminergic neurons associated with *SNCA* expression. In day 1 adult flies, dopaminergic neuron numbers in the PAM cluster showed no significant difference between genotypes (Figure 5G). In contrast, 12-day-old flies expressing *SNCA* showed a significantly stronger reduction of dopaminergic neurons than those expressing only *EGFP* RNAi or *skd/Med13* RNAi. *SNCA*-expressing flies that were fed DFO had similar numbers of dopaminergic neurons as those expressing only *EGFP* RNAi, thus exhibiting a strong rescue of neurodegeneration by DFO. Interestingly, this rescue was not seen in flies co-expressing *SNCA* and *skd/Med13* RNAi, indicating that the neuroprotective action of DFO is dependent on skd/*Med13* function. Dopaminergic neurons in the optic lobe showed similar effects of the above genotypes and drug treatment (Figure S5L). Since Sima/Hif is upregulated by DFO, the *skd/Med13*-dependent protective action of DFO is consistent with the possibility that *sima/Hif* exerts its neuroprotective function in a *skd/Med13*-dependent manner.

In summary, *sima/Hif* is induced in response to *SNCA* expression and is required cell autonomously for neuroprotection. Furthermore, DFO upregulates Sima/Hif in fly brains and suppresses neurodegeneration in a *skd/Med13*-dependent manner. This is consistent with how HIF1A interacts with the Mediator kinase module in mammals to induce transcription of genes encoding glycolytic enzymes.[62,65]

MED13 induction upregulates glycolytic enzymes and is neuroprotective in *SNCA*-overexpressing mice

To determine whether the induction of MED13 and glycolytic enzymes by *SNCA* overexpression is conserved between flies and mice, we compared homozygous transgenic mice expressing human *SNCA* with the A53T mutation (Tg) and non-transgenic controls (non-Tg). This PD mouse model has been reported to show human α-syn expression in western blots, α-syn pathology in immunohistochemistry, and motor phenotypes at 2–3, 7–8,

(E) Detection of glutathione oxidation status expressing cyto-Grx1-roGFP2 in PR synapses using *Rh1-GAL4* suggests a synergistic increase in GSSG:GSH ratio when *SNCA* expression is combined with *Med13* knockdown.

Data are plotted as means with SDs. Each point in (A), (B), and (D) represents data from one fly. n ≥ 25, 25, 40, 22, and 13 for (A), (B), (C), (D), and (E), respectively. Analyzed with two-way ANOVA followed by Tukey's multiple comparisons test in (C) and (E) and with Kruskal-Wallis test followed by Dunn's multiple comparisons test in (B) and (D). *p < 0.05, **p < 0.01, ***p < 0.001, and ****p < 0.0001. Scale bars indicate 3 μm in (A), 5 μm in (D), and 10 μm in (C) and (E).

See also Figure S4.

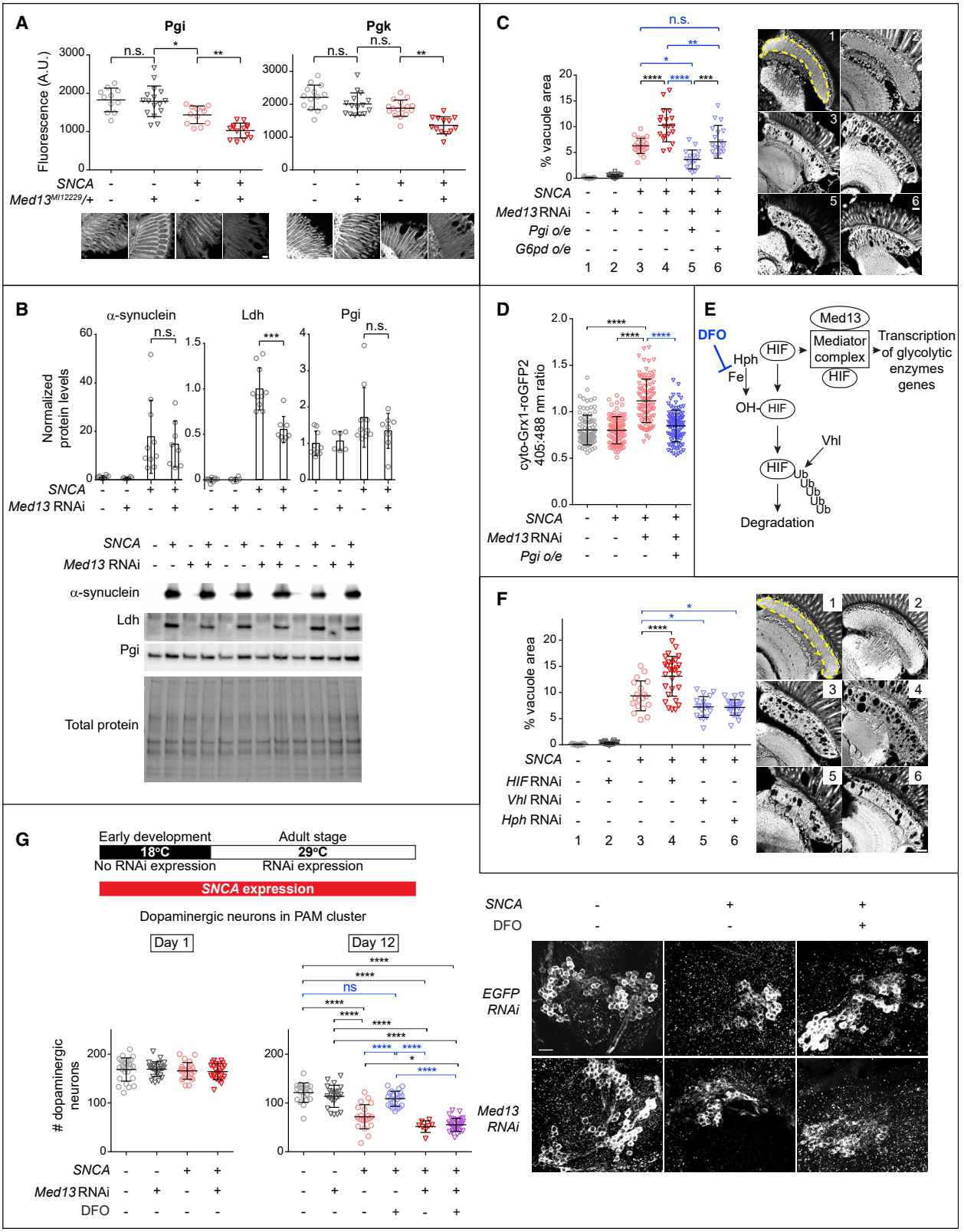

(legend on next page)

and 8–9 months of age, respectively.[83] In our hands, 3-month-old Tg mice showed an upregulation of MED13 in both cortex and midbrain compared with non-Tg controls; this difference persisted in the 6-month-old cortex but was reversed in the 6-month-old midbrain and disappeared in the 18-month-old cortex and midbrain (Figures 6A, 6B, and S6A). In 3-month-old mice, PGI, PGK, and LDH were upregulated in both cortex and midbrain of Tg mice compared with non-Tg controls, while these differences in glycolytic enzymes were either absent or reversed in 6- and 18-month-old mice. We also observed similar changes in spinal cord and brainstem (Figures S6B and S6C).

To determine whether HIF1A is upregulated in Tg mice, we performed immunohistochemistry (Figures 6C, 6D, and S6D). In the substantia nigra, dopaminergic (TH^+) neurons showed increased punctate HIF1A staining in Tg mice compared with non-Tg controls at 3 and 6 months old. In addition, in the brainstem and ventral spinal cord, $NeuN^+$ neurons showed increased HIF1A staining in Tg versus non-Tg mice at both time points. Therefore, overexpression of human *SNCA* in flies and mice neurons has similar effects on the expression of Med13, glycolytic enzymes, and HIF1A.

The conserved upregulation of MED13 and glycolytic enzymes prompted us to ask if knocking down *MED13* in Tg mice would prevent the upregulation of glycolytic enzymes. Five-month-old mice were subjected to unilateral injection of a short hairpin RNA (shRNA) targeting *MED13* in the substantia nigra and sacrificed 6 weeks postinjection (see STAR Methods). Consistent with western blot data (Figure 6), MED13 staining was higher in Tg mice compared with controls (Figures 7A and 7E); in both genotypes, *MED13* shRNA attenuated MED13 immunofluorescence by 50% or more when compared with the non-injected side. Interestingly, the levels of LDH and PGI in Tg mice, but not in non-Tg controls, were significantly reduced by *MED13* shRNA injection (Figures 7B, 7C, 7F, and 7G). PGK levels were reduced by *MED13* shRNA in both Tg mice and controls (Figures 7D and 7H). Injection of control adeno-associated virus (AAV) did not affect expression of all four proteins examined (Figures 7A–7H). Therefore, consistent with data from flies, MED13 is required for the upregulation of some glycolytic enzymes in response to *SNCA* overexpression.

To test the neuroprotective function of MED13, we quantified substantia nigra dopaminergic neurons. Control virus did not affect the number of TH^+ neurons in either non-Tg control or Tg mice (Figures S7A and S7B). In Tg mice, *MED13* shRNA injection led to a significant decrease of TH^+ neurons in the injected side compared with the non-injected side; similarly, injection of *MED13* shRNA led to reduced number of TH^+ neurons compared with injection of control virus. Interestingly, the reduction of TH^+ neurons by *MED13* knockdown was only seen in Tg mice and not in non-Tg control mice, suggesting a synergy between *MED13* knockdown and *SNCA* overexpression.

We further examined α-syn accumulation and mitochondrial morphology in TH^+ neurons in the substantia nigra (Figures S7C–S7E). Accumulation of human α-syn protein was not different between injected and uninjected tissue and was not different between *MED13* shRNA and control virus treatment. In contrast, mitochondrial aspect ratio was significantly reduced in Tg compared with non-Tg substantia nigra. In addition, *MED13* knockdown reduced mitochondrial aspect ratios in both non-Tg and Tg mice. Therefore, both human *SNCA* expression and *MED13* knockdown were associated with less elongated mitochondrial morphology, but *MED13* knockdown did not cause accumulation of α-syn protein.

Hence, in Tg mice at a relatively early stage of disease progression, *MED13* knockdown dampened the upregulation of glycolytic enzymes and reduced the number of substantia nigra dopaminergic neurons in an *SNCA*-dependent manner. In addition, *MED13* knockdown altered mitochondrial morphology without changing levels of α-syn.

DISCUSSION

To further our understanding of mechanisms underlying synucleinopathy, we conducted a screen for genetic modifiers of *SNCA* in *Drosophila* and identified 12 genes, all of which have human orthologs (Figure 1E). Notably, *MED13* and *CDC27* are

Figure 5. *Drosophila* Hif pathway and glycolysis are protective against *SNCA*-associated neurodegeneration

(A) A combination of *SNCA* expression and $Med13^{MI12229}$ heterozygosity reduced protein levels of Pgi (left) and Pgk (right) in the retina but either genetic manipulation on its own did not. *SNCA* was expressed using the PR-specific *Rh1-GAL4* driver, and flies were 14 days old. See also Figure S5B.

(B) *Med13* conditional knockdown with *HMS01305* RNAi in all neurons in adult flies dampened the induction of Ldh by *SNCA*; Pgi showed a slight but non-significant reduction. Levels of α-syn, Ldh, and Pgi were normalized to total protein levels. Flies were incubated at 25°C during larval development and at 29°C for 21 days after eclosion to induce expression using the *elav-GAL4 Tub-GAL80^{ts}* conditional driver.

(C) Co-expressing *Pgi* or *G6pd* with *SNCA* and *Med13* RNAi in PR neurons partially suppressed neurodegeneration to levels lower than *SNCA* expression alone.

(D) Cyto-Grx1-roGFP2 expressed in PR synapses using *Rh1-GAL4* suggests a restoration of GSSG:GSH ratio when *Pgi* is overexpressed in conjunction with *SNCA*-expression and *skd*/*Med13* knockdown.

(E) A schematic diagram of regulatory relationship between Hph, Vhl, HIF, Med13, and glycolytic enzymes, which are common to both flies and humans.

(F) *Rh1-GAL4*-driven knockdown of *Hif*, *Vhl*, and *Hph* modulated *SNCA*-associated neurodegeneration in retina. *P{attP,y+,w3'}VIE-260B* was used as a genetic background control for RNAi strains targeting *Hif*, *Hph*, and *Vhl*. Representative paraffin sections of retina of different genotypes (right).

(G) *SNCA* expression, *Med13* knockdown, and 1 mM DFO treatment were tested for their effects on the survival of PAM cluster dopaminergic neurons. *SNCA* and *Med13* RNAi were expressed in all neurons using the combination of transgenes *elav-GAL4 Tub-GAL80^{ts}*; to avoid developmental lethality, expression was limited to adulthood by shifting flies from 18°C to 29°C upon eclosion (see STAR Methods).

Data are plotted as means with SDs. Each point represents data from one fly. (A), (C), and (G) were analyzed with one-way ANOVA followed by Tukey's multiple comparisons test. (D) was analyzed with Kruskal-Wallis test followed by Dunn's multiple comparisons test. (F) was analyzed with one-way ANOVA followed by Dunnet's multiple comparisons test. Pairwise comparisons in (C) were made using Mann-Whitney test. n $\geq$ 11, 6, 16, 93, 18, and 8–32 for (A), (B), (C), (D), (F), and (G), respectively. *p < 0.05, **p < 0.01, ***p < 0.001, and ****p < 0.0001, and ns indicates not significant. Scale bars indicate 20 μm in (A), (C), and (F) and 10 μm in (G).

See also Figure S5.

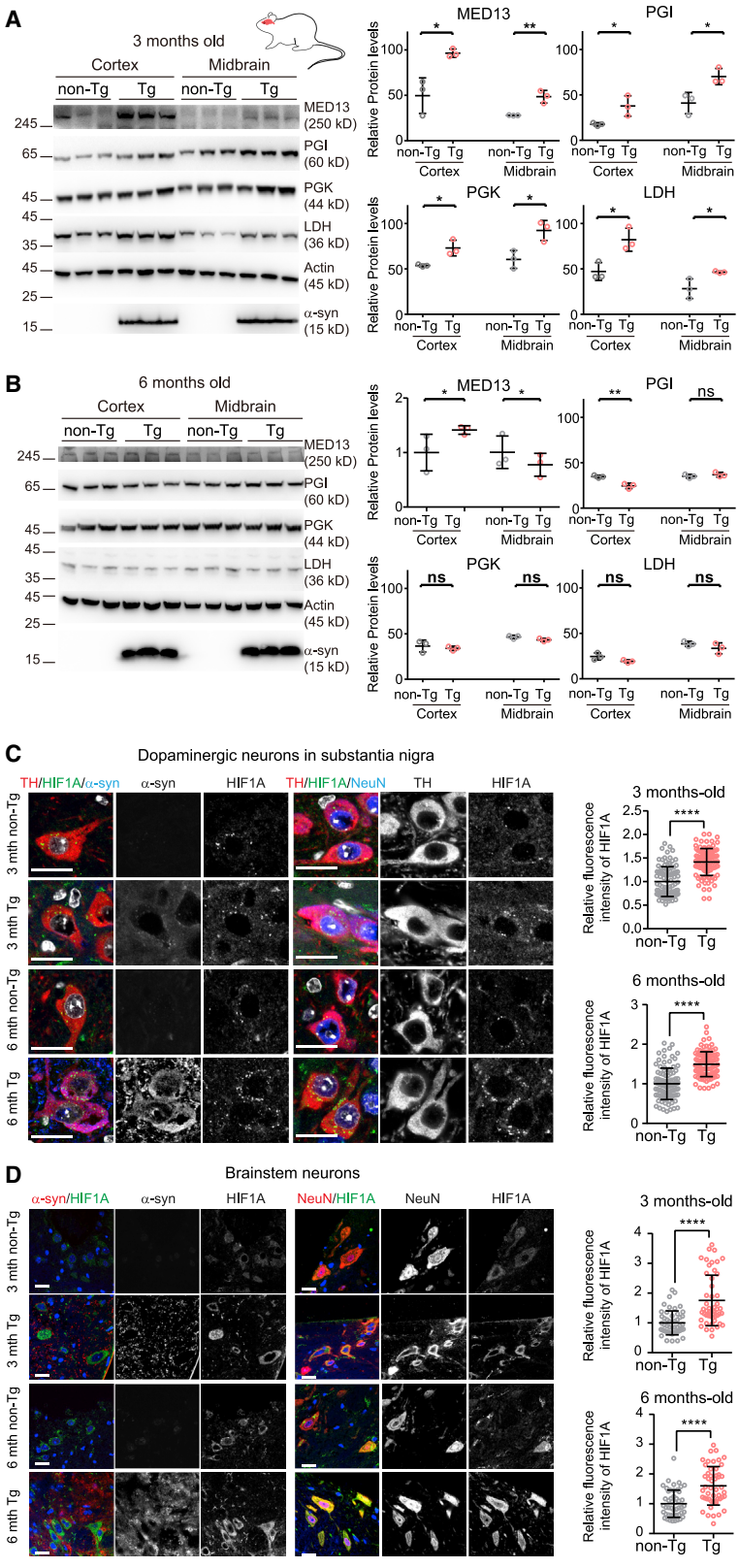

Figure 6. Levels of MED13 and glycolytic enzymes are altered dynamically by α-syn overexpression in mice

(A and B) Protein levels of MED13, Pgi, Pgk2, and LDHA in cortex and midbrain tissues of 3- (A) and 6-month-old (B) transgenic mice expressing human *SNCA.A53T* (Tg) and the non-transgenic controls (non-Tg). In 3 month olds, *SNCA* expression correlated with induction of MED13 and glycolytic enzymes, but in 6 month olds, only MED13 remained upregulated. Protein levels were normalized to actin. Each point represents data from one mouse.

(C and D) Images showing increased HIF1α staining in TH^+ neurons in substantia nigra (C) and $NeuN^+$ neurons in L4/5 ventral spinal cord (D).

(C) Substantia nigra slices were stained either with antibodies against TH, HIF1A, and α-syn (left) or TH, HIF1A, and NeuN (right). 100 TH^+ neurons from five mice were quantified for each genotype/time point.

(D) Brainstem slices were stained either with antibodies against α-syn and HIF1A (left) or NeuN and HIF1A (right). 50 $NeuN^+$ neurons from five mice were quantified for each genotype/time point.

Data are plotted as means with SDs. Comparisons were made using t tests. *p < 0.05, **p < 0.01, and ***p < 0.0001, and ns indicates not significant. Scale bars indicate 20 μm in (C) and (D).

See also Figure S6.

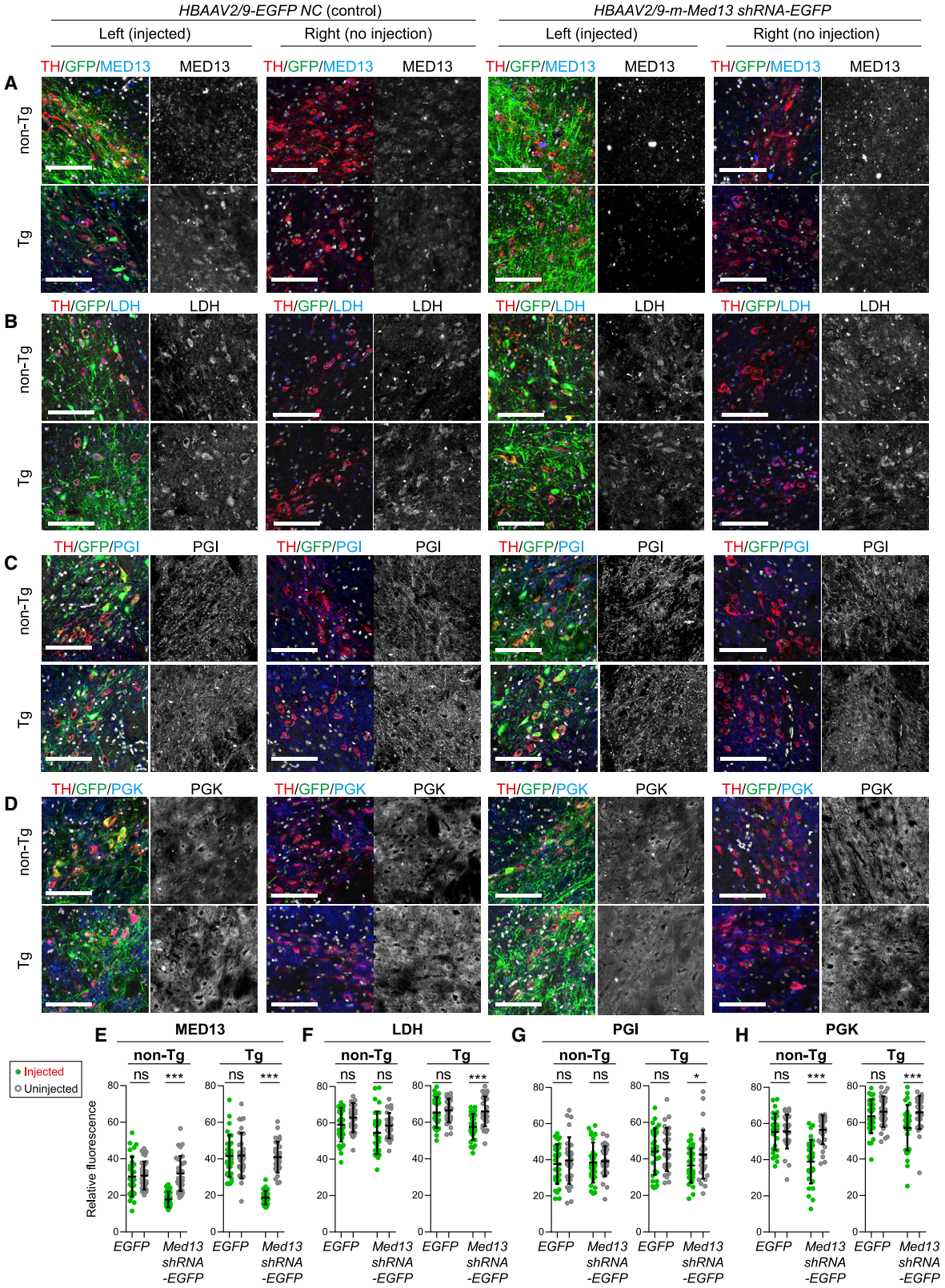

(legend on next page)

located near PD GWAS SNPs[17]; in particular, *MED13* has been independently implicated in PD in a transcriptome-wide association study (TWAS) based on human brain tissues.[84] *ABCB7*, *GARS1*, *COX20*, and *NDUFA9* underlie Mendelian mitochondrial disorders with neurological symptoms.[46,50,51,53] *CDC27*, *CDAN1*, *MTA1*, *MED13*, *RBPMS2*, and *NR1D1* are associated with polymorphisms implicated in human diseases by GWAS[17,47,48,52,54]; in particular, *NR1D1* and *CDAN1* are implicated for neurological disorders (multiple sclerosis and bipolar type 1, respectively). Hence, two-thirds of the *SNCA* modifiers have human orthologs with known associations with neurological disorders, suggesting that they are likely to be authentic modifiers of synucleinopathies.

While a large number of *SNCA* modifiers described in the literature modulate α-syn accumulation,[14,30,85] some, such as TRAP1, AP-2α, and Hsp70, do not.[86–88] Interestingly, all 12 modifiers do not affect levels of α-syn and pS129 (Figures 5B, S1E, and S7D). Compared with a screen that used α-syn accumulation as the primary screen criterion,[89] we used neurodegeneration and seem to have recovered a distinct set of modifiers. Alternatively, by examining the effect of mild (50% or less) reductions of gene functions, our screen may have revealed processes that are impaired before pathological α-syn accumulation occurs.

Among the *SNCA* modifier screens reported, *MED13* homologs have never been recovered.[14,26,35–37,85,86,90] However, a loss-of-function mutation in *skd*/*Med13* has been recovered as a dominant enhancer of neurodegeneration phenotypes associated with polyglutamine mutations in *ataxin 1* and *huntingtin*.[91] Interestingly, heterozygous mutations of *MED13* in humans have been found to underlie a rare neurodevelopmental disorder.[92] Taken together, the data on *MED13* heterozygosity in flies and humans are consistent with the idea that relatively modest perturbations of the levels of *MED13* function can increase the risk of neuropathology.

Activation of glycolytic genes by the Mediator kinase module has been demonstrated in non-neuronal cells,[62,65] but as far as we know, this is the first time *MED13* has been shown to be required for the full induction of glycolytic enzymes in differentiated neurons. A compensatory increase in glycolysis in response to mitochondrial disruption has been observed elsewhere and is thought to occur through the transcriptional activity of HIF1A.[93–97] Interestingly, previous studies have identified glycolysis as a modifier of PD models and brain aging, respectively.[27,68,98,99] Here, our data that *sima*/*Hif* and overexpression of *Pgi* and *Pfk* are protective against *SNCA*-associated neurodegeneration support the idea that compensatory glycolysis is neuroprotective (Figures 5C, 5F, and S5E). Ldh and lactate levels were strongly upregulated by *SNCA* (Figures 3E, S3F, and 6), suggesting that high levels of Ldh activity may generate NAD+ to keep glycolytic flux high (Figure 3B).[66] However, *Ldh* overexpression slightly worsened neurodegeneration in fly PR neurons (Figure S5F), consistent with too much and too little *Ldh* enhancing neurodegeneration and reducing lifespan.[100,101] Therefore, artificially increasing the level of *Pgi* and *Pfk*, but not *Ldh*, is protective.

We note that the regulation of MED13 and glycolytic enzymes evolve with age. In mice, the initial upregulation of MED13 and glycolytic enzymes at 3 months was attenuated by 6 months (Figures 6A and 6B), while this reversal did not occur in flies from larval to old adults (Figure 3), possibly because adult flies older than 4 weeks were not assessed. We note that flies undergo metabolic remodeling during metamorphosis between larval and adult stages,[102,103] which may explain the difference in progression of the MED13-glycolytic response toward *SNCA* expression compared with mice. On the other hand, the attenuation of glycolytic enzymes in Tg mice after an initial rise may suggest feedback mechanisms.

ATP generated by compensatory glycolysis in response to mitochondrial impairment is likely channeled toward GSH synthesis, as suggested by a previous study[104] (see also Figure 3B). Consistent with this idea, our data show a synergistic increase in GSSG:GSH ratio by combining *skd*/*Med13* RNAi and *SNCA* expression (Figure 4E) and restoration to normal levels by *Pgi* overexpression (Figure 5D). While artificially overexpressing *G6pd* was protective, *G6pd* was not induced by *SNCA* (Figures 5C and S3B); this suggests that the main endogenous response toward *SNCA* is to upregulate *de novo* GSH synthesis instead of recycling GSH from GSSG. Taken together, our data suggest that compensatory glycolysis is required for GSH production to counter mitochondria-related oxidative stress. However, further work is needed to test if neuroprotection by MED13 truly takes effect through glycolysis.

Our data on DFO suggest that the HIF pathway interacts with MED13 (Figures 5G and S5L). Interestingly, *EGLN3*/*Hph*, the human gene encoding the target of DFO, lies near SNPs associated with Alzheimer's disease,[105–108] and a non-synonymous polymorphism in a *HIF1A* coding exon is associated with late-onset PD.[109] Taken together, human genetics suggests that *MED13* and *HIF1A* are strong candidates as genetic modifiers of PD. In addition, our study also supports DFO, an FDA-approved drug, for further investigation as a candidate drug for PD.

Therefore, the genetic evidence suggests that enhancing glucose metabolism is a viable strategy for treating PD. Indeed, inhibitors of Hph/EGLN3 and glycolytic stimulators have been shown to ameliorate models of synucleinopathy.[68,110,111] In addition, exenatide, a glucagon-like peptide-1 receptor (GLP-1R) agonist, which increases brain glucose uptake,[112,113] has shown possible disease-modifying effects in clinical trials on PD.[114,115]

Figure 7. *MED13* is required for upregulation of glycolytic enzymes in PD mice

(A–D) Immunofluorescence images of substantia nigra from wild-type (WT) and PD mice injected with control and *Med13* shRNA only in the left substantia nigra, leaving the right side uninjected. Both control and *Med13* shRNA-containing viruses expressed EGFP. Sections were stained with Med13 (A), LDH (B), Pgi (C), and Pgk (D), respectively. Labels for TH and DNA are in red and white, respectively. Scale bar indicates 100 μm.

(E–H) Quantitation of Med13 (E), LDH (F), Pgi (G), and Pgk (H) intensity in left (injected) and right (uninjected) substantia nigra from WT and PD mice infused with control and *Med13* shRNA.

n = 15 images from 3 mice in each group. Data are plotted as means with SDs. Pairwise comparisons were performed using t tests. *$p < 0.05$ and ***$p < 0.001$, and ns indicates not significant.

Consistent with earlier efforts,[116,117] our study demonstrates that genetic modifiers can be used to identify disease-modifying pathways and candidate drugs. There have been efforts in yeast, worms, flies, mice, and humans to identify modifiers of *SNCA*,[24,26,28,30–38,87,118] uncovering multiple independent pathways. As perturbations of independent pathways that converge on the same processes can potentially produce additive or synergistic effects,[20] combining drugs targeting distinct pathways can potentially produce therapeutic effects stronger than a mono-therapeutic approach. Hence, further investigations into the diverse modifiers of synucleinopathy may uncover opportunities for effective combinatorial drug therapies.

Limitations of the study

First, we have not attempted gain-of-function *MED13* experiments to test for suppression of neurodegeneration due to concerns that overexpressing MED13 alone could ectopically disrupt the stoichiometry of the multi-subunit Mediator complex; indeed, overexpression of *skd/Med13* in flies causes lethality and developmental defects.[63] Second, although the lack of PH3 and PCNA staining suggests that reduced *skd/Med13* function did not elicit obvious cell cycle re-entry in *SNCA*-expressing fly neurons, the short duration of *Drosophila* cell cycle could be challenging to observe.[119] Third, while the *skd/Med13* dependence of the DFO treatment suggests that Hph/EGLN3 and Vhl are upstream of *Med13*, we acknowledge that DFO may act through alternative targets. Fourth, we note that our data showing lower numbers of substantia nigra dopaminergic neurons in Tg mice compared with non-Tg controls may contradict the absence of synucleinopathy in the original description of the Tg mice,[83] although we note that (1) similar reductions have been previously reported[120–122] and (b) synuclein pathology and nigral neuron loss do not show positive correlation in human PD brain samples.[123,124]

STAR★METHODS

Detailed methods are provided in the online version of this paper and include the following:

- KEY RESOURCES TABLE
- RESOURCE AVAILABILITY
  - Lead contact
  - Materials availability
  - Data and code availability
- EXPERIMENTAL MODEL AND SUBJECT DETAILS
  - Fly stocks and transgenes
  - Mouse model
- METHOD DETAILS
  - Genetic screen for *SNCA* dominant modifier in *Drosophila*
  - Temporal control of RNAi expression in *SNCA*-expressing flies using the TARGET system
  - Whole mount immunohistochemistry of fly brains
  - Imaging of genetically-encoded biosensors in fly neurons
  - Quantitative real-time PCR of fly transcripts
  - Western blot analysis of fly tissue lysates
  - Western blot analysis of mouse brain lysates
  - Stereotaxic injection of adeno-associated virus (AAV) with short hairpin RNA (shRNA) and TH-positive cell counting
  - Immunohistochemistry of mouse brain
  - Analysis of mitochondrial aspect ratio in mouse brain slices
- QUANTIFICATION AND STATISTICAL ANALYSIS
  - Quantification of *Drosophila* climbing assay using the FlySpotter code
  - Additional image analysis and quantification
  - Statistical analyses

SUPPLEMENTAL INFORMATION

Supplemental information can be found online at https://doi.org/10.1016/j.celrep.2022.111852.

ACKNOWLEDGMENTS

We thank Tee Chuan Sia, Leo Chan, Wei Jun Tan, Cassandra Ngoh, Judy M. Ho, Lyn Yong, Shintaro Ng, Ivan Phanada, Joel Ng, G. Suthershinii, and Deborah Loh for technical assistance. We also express gratitude to Hugo Bellen, Josh Shulman, Jessica Treisman, Mel Feany, Horng-Dar Wang, Pablo Wappner, David Glover, and Yu Cai for generously providing reagents. T.-W.K. was supported by National Research Foundation fellowship NRF-NRFF2015-06. M.R. and K.L.L. were supported by National Medical Research Council Large Collaborative Grant – SPARK2 (L.K.L.). Y.Y. was supported by National Natural Science Foundation of China 82001200 and J.Z. was supported by 81571226, 82020108012, and 81671187.

AUTHOR CONTRIBUTIONS

T.-W.K., M.R., and Y.Y. conceived and designed the study. M.R., Y.Y., K.H.Y.H., L.Y.N., C.Y.-Y.C., R.M.Q.L., and T.-W.K. conducted the experiments. Y.T.N. performed variant analysis of the fly mutants. S.G.-S. wrote the code for analyzing fly behavioral assay. M.R., Y.Y., K.H.Y.H., C.Y.-Y.C., R.M.Q.L., K.L.L., J.Z., and T.-W.K. were responsible for data interpretation. T.-W.K., M.R., and Y.Y. prepared the manuscript with contributions from other authors.

DECLARATION OF INTERESTS

The authors declare no competing interests.

Received: April 6, 2022
Revised: October 4, 2022
Accepted: November 29, 2022
Published: December 20, 2022

REFERENCES

1. Li, W.-W., Yang, R., Guo, J.-C., Ren, H.-M., Zha, X.-L., Cheng, J.-S., and Cai, D.-F. (2007). Localization of alpha-synuclein to mitochondria within midbrain of mice. Neuroreport *18*, 1543–1546. https://doi.org/10.1097/WNR.0b013e3282f03db4.
2. Maroteaux, L., Campanelli, J.T., and Scheller, R.H. (1988). Synuclein: a neuron-specific protein localized to the nucleus and presynaptic nerve terminal. J. Neurosci. *8*, 2804–2815.
3. Bendor, J.T., Logan, T.P., and Edwards, R.H. (2013). The function of α-synuclein. Neuron *79*, 1044–1066. https://doi.org/10.1016/j.neuron.2013.09.004.
4. Theillet, F.-X., Binolfi, A., Bekei, B., Martorana, A., Rose, H.M., Stuiver, M., Verzini, S., Lorenz, D., van Rossum, M., Goldfarb, D., and Selenko, P.

(2016). Structural disorder of monomeric α-synuclein persists in mammalian cells. Nature *530*, 45–50. https://doi.org/10.1038/nature16531.

5. Wang, W., Perovic, I., Chittuluru, J., Kaganovich, A., Nguyen, L.T.T., Liao, J., Auclair, J.R., Johnson, D., Landeru, A., Simorellis, A.K., et al. (2011). A soluble α-synuclein construct forms a dynamic tetramer. Proc. Natl. Acad. Sci. USA *108*, 17797–17802. https://doi.org/10.1073/pnas.1113260108.
6. Winner, B., Jappelli, R., Maji, S.K., Desplats, P.A., Boyer, L., Aigner, S., Hetzer, C., Loher, T., Vilar, M., Campioni, S., et al. (2011). In vivo demonstration that alpha-synuclein oligomers are toxic. Proc. Natl. Acad. Sci. USA *108*, 4194–4199. https://doi.org/10.1073/pnas.1100976108.
7. Volpicelli-Daley, L.A., Luk, K.C., Patel, T.P., Tanik, S.A., Riddle, D.M., Stieber, A., Meaney, D.F., Trojanowski, J.Q., and Lee, V.M.-Y. (2011). Exogenous α-synuclein fibrils induce Lewy body pathology leading to synaptic dysfunction and neuron death. Neuron *72*, 57–71. https://doi.org/10.1016/j.neuron.2011.08.033.
8. Cremades, N., Cohen, S.I.A., Deas, E., Abramov, A.Y., Chen, A.Y., Orte, A., Sandal, M., Clarke, R.W., Dunne, P., Aprile, F.A., et al. (2012). Direct observation of the interconversion of normal and toxic forms of α-synuclein. Cell *149*, 1048–1059. https://doi.org/10.1016/j.cell.2012.03.037.
9. Spillantini, M.G., Schmidt, M.L., Lee, V.M., Trojanowski, J.Q., Jakes, R., and Goedert, M. (1997). α-Synuclein in Lewy bodies. Nature *388*, 839–840. https://doi.org/10.1038/42166.
10. Peng, C., Gathagan, R.J., Covell, D.J., Medellin, C., Stieber, A., Robinson, J.L., Zhang, B., Pitkin, R.M., Olufemi, M.F., Luk, K.C., et al. (2018). Cellular milieu imparts distinct pathological α-synuclein strains in α-synucleinopathies. Nature *557*, 558–563. https://doi.org/10.1038/s41586-018-0104-4.
11. Lang, A., Dassler, E., Milenkovic, I., Lutz, M.I., and Kovacs, G.G. (2021). Variable expression of mitochondrial complex IV in the course of nigral intracellular accumulation of α-synuclein. Parkinsonism Relat. Disord. *90*, 57–61. https://doi.org/10.1016/j.parkreldis.2021.08.001.
12. Ludtmann, M.H.R., Angelova, P.R., Horrocks, M.H., Choi, M.L., Rodrigues, M., Baev, A.Y., Berezhnov, A.V., Yao, Z., Little, D., Banushi, B., et al. (2018). α-synuclein oligomers interact with ATP synthase and open the permeability transition pore in Parkinson's disease. Nat. Commun. *9*, 2293. https://doi.org/10.1038/s41467-018-04422-2.
13. Nakamura, K., Nemani, V.M., Azarbal, F., Skibinski, G., Levy, J.M., Egami, K., Munishkina, L., Zhang, J., Gardner, B., Wakabayashi, J., et al. (2011). Direct membrane association drives mitochondrial fission by the Parkinson disease-associated protein α-synuclein. J. Biol. Chem. *286*, 20710–20726. https://doi.org/10.1074/jbc.M110.213538.
14. Ordonez, D.G., Lee, M.K., and Feany, M.B. (2018). α-Synuclein induces mitochondrial dysfunction through spectrin and the actin cytoskeleton. Neuron *97*, 108–124.e6. https://doi.org/10.1016/j.neuron.2017.11.036.
15. Boot, B.P., Orr, C.F., Ahlskog, J.E., Ferman, T.J., Roberts, R., Pankratz, V.S., Dickson, D.W., Parisi, J., Aakre, J.A., Geda, Y.E., et al. (2013). Risk factors for dementia with Lewy bodies: a case-control study. Neurology *81*, 833–840. https://doi.org/10.1212/WNL.0b013e3182a2cbd1.
16. Kalia, L.V., and Lang, A.E. (2015). Parkinson's disease. Lancet *386*, 896–912. https://doi.org/10.1016/s0140-6736(14)61393-3.
17. Nalls, M.A., Blauwendraat, C., Vallerga, C.L., Heilbron, K., Bandres-Ciga, S., Chang, D., Tan, M., Kia, D.A., Noyce, A.J., Xue, A., et al. (2019). Identification of novel risk loci, causal insights, and heritable risk for Parkinson's disease: a meta-analysis of genome-wide association studies. Lancet Neurol. *18*, 1091–1102. https://doi.org/10.1016/S1474-4422(19)30320-5.
18. Chia, R., Sabir, M.S., Bandres-Ciga, S., Saez-Atienzar, S., Reynolds, R.H., Gustavsson, E., Walton, R.L., Ahmed, S., Viollet, C., Ding, J., et al. (2021). Genome sequencing analysis identifies new loci associated with Lewy body dementia and provides insights into its genetic architecture. Nat. Genet. *53*, 294–303. https://doi.org/10.1038/s41588-021-00785-3.
19. Jansen, I.E., Ye, H., Heetveld, S., Lechler, M.C., Michels, H., Seinstra, R.I., Lubbe, S.J., Drouet, V., Lesage, S., Majounie, E., et al. (2017). Discovery and functional prioritization of Parkinson's disease candidate genes from large-scale whole exome sequencing. Genome Biol. *18*, 22. https://doi.org/10.1186/s13059-017-1147-9.
20. Fang, G., Wang, W., Paunic, V., Heydari, H., Costanzo, M., Liu, X., Liu, X., VanderSluis, B., Oately, B., Steinbach, M., et al. (2019). Discovering genetic interactions bridging pathways in genome-wide association studies. Nat. Commun. *10*, 4274. https://doi.org/10.1038/s41467-019-12131-7.
21. Zuk, O., Hechter, E., Sunyaev, S.R., and Lander, E.S. (2012). The mystery of missing heritability: genetic interactions create phantom heritability. Proc. Natl. Acad. Sci. USA *109*, 1193–1198. https://doi.org/10.1073/pnas.1119675109.
22. Genetic Modifiers of Huntington's Disease GeM-HD Consortium (2015). Identification of genetic factors that modify clinical onset of Huntington's disease. Cell *162*, 516–526. https://doi.org/10.1016/j.cell.2015.07.003.
23. Lai, D., Alipanahi, B., Fontanillas, P., Schwantes-An, T.-H., Aasly, J., Alcalay, R.N., Beecham, G.W., Berg, D., Bressman, S., Brice, A., et al. (2021). Genomewide association studies of LRRK2 modifiers of Parkinson's disease. Ann. Neurol. *90*, 76–88. https://doi.org/10.1002/ana.26094.
24. Blauwendraat, C., Reed, X., Krohn, L., Heilbron, K., Bandres-Ciga, S., Tan, M., Gibbs, J.R., Hernandez, D.G., Kumaran, R., Langston, R., et al. (2020). Genetic modifiers of risk and age at onset in GBA associated Parkinson's disease and Lewy body dementia. Brain *143*, 234–248. https://doi.org/10.1093/brain/awz350.
25. Brown, E.E., Blauwendraat, C., Trinh, J., Rizig, M., Nalls, M.A., Leveille, E., Ruskey, J.A., Jonvik, H., Tan, M.M., Bandres-Ciga, S., et al. (2021). Analysis of DNM3 and VAMP4 as genetic modifiers of LRRK2 Parkinson's disease. Neurobiol. Aging *97*, 148.e17–148.e24. https://doi.org/10.1016/j.neurobiolaging.2020.07.002.
26. Gitler, A.D., Chesi, A., Geddie, M.L., Strathearn, K.E., Hamamichi, S., Hill, K.J., Caldwell, K.A., Caldwell, G.A., Cooper, A.A., Rochet, J.-C., and Lindquist, S. (2009). Alpha-synuclein is part of a diverse and highly conserved interaction network that includes PARK9 and manganese toxicity. Nat. Genet. *41*, 308–315. https://doi.org/10.1038/ng.300.
27. Knight, A.L., Yan, X., Hamamichi, S., Ajjuri, R.R., Mazzulli, J.R., Zhang, M.W., Daigle, J.G., Zhang, S., Borom, A.R., Roberts, L.R., et al. (2014). The glycolytic enzyme, GPI, is a functionally conserved modifier of dopaminergic neurodegeneration in Parkinson's models. Cell Metab. *20*, 145–157. https://doi.org/10.1016/j.cmet.2014.04.017.
28. Brahmachari, S., Ge, P., Lee, S.H., Kim, D., Karuppagounder, S.S., Kumar, M., Mao, X., Shin, J.H., Lee, Y., Pletnikova, O., et al. (2016). Activation of tyrosine kinase c-Abl contributes to α-synuclein-induced neurodegeneration. J. Clin. Invest. *126*, 2970–2988. https://doi.org/10.1172/JCI85456.
29. Li, H., Wu, S., Ma, X., Li, X., Cheng, T., Chen, Z., Wu, J., Lv, L., Li, L., Xu, L., et al. (2021). Co-Editing PINK1 and DJ-1 genes via adeno-associated virus-delivered CRISPR/Cas9 system in adult monkey brain elicits classical parkinsonian phenotype. Neurosci. Bull. *37*, 1271–1288. https://doi.org/10.1007/s12264-021-00732-6.
30. Fishbein, I., Kuo, Y.-M., Giasson, B.I., and Nussbaum, R.L. (2014). Augmentation of phenotype in a transgenic Parkinson mouse heterozygous for a Gaucher mutation. Brain *137*, 3235–3247. https://doi.org/10.1093/brain/awu291.
31. Barone, M.C., Sykiotis, G.P., and Bohmann, D. (2011). Genetic activation of Nrf2 signaling is sufficient to ameliorate neurodegenerative phenotypes in a Drosophila model of Parkinson's disease. Dis. Model. Mech. *4*, 701–707. https://doi.org/10.1242/dmm.007575.
32. Du, G., Liu, X., Chen, X., Song, M., Yan, Y., Jiao, R., and Wang, C.-C. (2010). Drosophila histone deacetylase 6 protects dopaminergic neurons against alpha-synuclein toxicity by promoting inclusion formation. Mol. Biol. Cell *21*, 2128–2137. https://doi.org/10.1091/mbc.e10-03-0200.

33. Suzuki, M., Fujikake, N., Takeuchi, T., Kohyama-Koganeya, A., Nakajima, K., Hirabayashi, Y., Wada, K., and Nagai, Y. (2015). Glucocerebrosidase deficiency accelerates the accumulation of proteinase K-resistant α-synuclein and aggravates neurodegeneration in a Drosophila model of Parkinson's disease. Hum. Mol. Genet. *24*, 6675–6686. https://doi.org/10.1093/hmg/ddv372.

34. Whitworth, A.J., Theodore, D.A., Greene, J.C., Benes, H., Wes, P.D., and Pallanck, L.J. (2005). Increased glutathione S-transferase activity rescues dopaminergic neuron loss in a Drosophila model of Parkinson's disease. Proc. Natl. Acad. Sci. USA *102*, 8024–8029. https://doi.org/10.1073/pnas.0501078102.

35. Hamamichi, S., Rivas, R.N., Knight, A.L., Cao, S., Caldwell, K.A., and Caldwell, G.A. (2008). Hypothesis-based RNAi screening identifies neuroprotective genes in a Parkinson's disease model. Proc. Natl. Acad. Sci. USA *105*, 728–733. https://doi.org/10.1073/pnas.0711018105.

36. van Ham, T.J., Thijssen, K.L., Breitling, R., Hofstra, R.M.W., Plasterk, R.H.A., and Nollen, E.A.A. (2008). C. elegans model identifies genetic modifiers of alpha-synuclein inclusion formation during aging. PLoS Genet. *4*, e1000027. https://doi.org/10.1371/journal.pgen.1000027.

37. Tardiff, D.F., Jui, N.T., Khurana, V., Tambe, M.A., Thompson, M.L., Chung, C.Y., Kamadurai, H.B., Kim, H.T., Lancaster, A.K., Caldwell, K.A., et al. (2013). Yeast reveal a "druggable" Rsp5/Nedd4 network that ameliorates α-synuclein toxicity in neurons. Science *342*, 979–983. https://doi.org/10.1126/science.1245321.

38. Lin, G., Lee, P.-T., Chen, K., Mao, D., Tan, K.L., Zuo, Z., Lin, W.-W., Wang, L., and Bellen, H.J. (2018). Phospholipase PLA2G6, a parkinsonism-associated gene, affects Vps26 and Vps35, retromer function, and ceramide levels, similar to α-synuclein gain. Cell Metab. *28*, 605–618.e6. https://doi.org/10.1016/j.cmet.2018.05.019.

39. Matsui, H., Gavinio, R., Asano, T., Uemura, N., Ito, H., Taniguchi, Y., Kobayashi, Y., Maki, T., Shen, J., Takeda, S., et al. (2013). PINK1 and Parkin complementarily protect dopaminergic neurons in vertebrates. Hum. Mol. Genet. *22*, 2423–2434. https://doi.org/10.1093/hmg/ddt095.

40. Yamamoto, S., Jaiswal, M., Charng, W.-L., Gambin, T., Karaca, E., Mirzaa, G., Wiszniewski, W., Sandoval, H., Haelterman, N.A., Xiong, B., et al. (2014). A Drosophila genetic resource of mutants to study mechanisms underlying human genetic diseases. Cell *159*, 200–214. https://doi.org/10.1016/j.cell.2014.09.002.

41. Zhai, R.G., Hiesinger, P.R., Koh, T.-W., Verstreken, P., Schulze, K.L., Cao, Y., Jafar-Nejad, H., Norga, K.K., Pan, H., Bayat, V., et al. (2003). Mapping Drosophila mutations with molecularly defined P element insertions. Proc. Natl. Acad. Sci. USA *100*, 10860–10865.

42. Cook, R.K., Christensen, S.J., Deal, J.A., Coburn, R.A., Deal, M.E., Gresens, J.M., Kaufman, T.C., and Cook, K.R. (2012). The generation of chromosomal deletions to provide extensive coverage and subdivision of the Drosophila melanogaster genome. Genome Biol. *13*, R21. https://doi.org/10.1186/gb-2012-13-3-r21.

43. Treisman, J. (2001). Drosophila homologues of the transcriptional coactivation complex subunits TRAP240 and TRAP230 are required for identical processes in eye-antennal disc development. Development *128*, 603–615.

44. Buniello, A., MacArthur, J.A.L., Cerezo, M., Harris, L.W., Hayhurst, J., Malangone, C., McMahon, A., Morales, J., Mountjoy, E., Sollis, E., et al. (2019). The NHGRI-EBI GWAS Catalog of published genome-wide association studies, targeted arrays and summary statistics 2019. Nucleic Acids Res. *47*, D1005–D1012. https://doi.org/10.1093/nar/gky1120.

45. OMIM®. Online Mendelian Inheritance in Man. https://omim.org/.

46. Allikmets, R., Raskind, W.H., Hutchinson, A., Schueck, N.D., Dean, M., and Koeller, D.M. (1999). Mutation of a putative mitochondrial iron transporter gene (ABC7) in X-linked sideroblastic anemia and ataxia (XLSA/A). Hum. Mol. Genet. *8*, 743–749. https://doi.org/10.1093/hmg/8.5.743.

47. Stahl, E.A., Breen, G., Forstner, A.J., McQuillin, A., Ripke, S., Trubetskoy, V., Mattheisen, M., Wang, Y., Coleman, J.R.I., Gaspar, H.A., et al. (2019). Genome-wide association study identifies 30 loci associated with bipolar disorder. Nat. Genet. *51*, 793–803. https://doi.org/10.1038/s41588-019-0397-8.

48. Frenkel, S., Bernstein, C.N., Sargent, M., Kuang, Q., Jiang, W., Wei, J., Thiruvahindrapuram, B., Spriggs, E., Scherer, S.W., and Hu, P. (2019). Genome-wide analysis identifies rare copy number variations associated with inflammatory bowel disease. PLoS One *14*, e0217846. https://doi.org/10.1371/journal.pone.0217846.

49. Makino, N., Yamato, T., Inoue, H., Furukawa, T., Abe, T., Yokoyama, T., Yatsuoka, T., Fukushige, S., Orikasa, S., Takahashi, T., and Horii, A. (2001). Isolation and characterization of the human gene homologous to the Drosophila headcase (hdc) gene in chromosome bands 6q23-q24, a region of common deletion in human pancreatic cancer. DNA Seq. *11*, 547–553. https://doi.org/10.3109/10425170109041340.

50. Griffin, L.B., Sakaguchi, R., McGuigan, D., Gonzalez, M.A., Searby, C., Züchner, S., Hou, Y.-M., and Antonellis, A. (2014). Impaired function is a common feature of neuropathy-associated glycyl-tRNA synthetase mutations. Hum. Mutat. *35*, 1363–1371. https://doi.org/10.1002/humu.22681.

51. Szklarczyk, R., Wanschers, B.F.J., Nijtmans, L.G., Rodenburg, R.J., Zschocke, J., Dikow, N., van den Brand, M.A.M., Hendriks-Franssen, M.G.M., Gilissen, C., Veltman, J.A., et al. (2013). A mutation in the FAM36A gene, the human ortholog of COX20, impairs cytochrome c oxidase assembly and is associated with ataxia and muscle hypotonia. Hum. Mol. Genet. *22*, 656–667. https://doi.org/10.1093/hmg/dds473.

52. van der Harst, P., and Verweij, N. (2018). Identification of 64 novel genetic loci provides an expanded view on the genetic architecture of coronary artery disease. Circ. Res. *122*, 433–443. https://doi.org/10.1161/CIRCRESAHA.117.312086.

53. van den Bosch, B.J.C., Gerards, M., Sluiter, W., Stegmann, A.P.A., Jongen, E.L.C., Hellebrekers, D.M.E.I., Oegema, R., Lambrichs, E.H., Prokisch, H., Danhauser, K., et al. (2012). Defective NDUFA9 as a novel cause of neonatally fatal complex I disease. J. Med. Genet. *49*, 10–15. https://doi.org/10.1136/jmedgenet-2011-100466.

54. International Multiple Sclerosis Genetics Consortium (2019). Multiple sclerosis genomic map implicates peripheral immune cells and microglia in susceptibility. Science *365*, eaav7188. https://doi.org/10.1126/science.aav7188.

55. Chen, L., and Feany, M.B. (2005). Alpha-synuclein phosphorylation controls neurotoxicity and inclusion formation in a Drosophila model of Parkinson disease. Nat. Neurosci. *8*, 657–663. https://doi.org/10.1038/nn1443.

56. Grenn, F.P., Kim, J.J., Makarious, M.B., Iwaki, H., Illarionova, A., Brolin, K., Kluss, J.H., Schumacher-Schuh, A.F., Leonard, H., Faghri, F., et al. (2020). The Parkinson's disease genome-wide association study locus browser. Mov. Disord. *35*, 2056–2067. https://doi.org/10.1002/mds.28197.

57. Wang, D., Liu, S., Warrell, J., Won, H., Shi, X., Navarro, F.C.P., Clarke, D., Gu, M., Emani, P., Yang, Y.T., et al. (2018). Comprehensive functional genomic resource and integrative model for the human brain. Science *362*, eaat8464. https://doi.org/10.1126/science.aat8464.

58. Qi, T., Wu, Y., Zeng, J., Zhang, F., Xue, A., Jiang, L., Zhu, Z., Kemper, K., Yengo, L., Zheng, Z., et al. (2018). Identifying gene targets for brain-related traits using transcriptomic and methylomic data from blood. Nat. Commun. *9*, 2282. https://doi.org/10.1038/s41467-018-04558-1.

59. Sieberts, S.K., Perumal, T.M., Carrasquillo, M.M., Allen, M., Reddy, J.S., Hoffman, G.E., Dang, K.K., Calley, J., Ebert, P.J., Eddy, J., et al. (2020). Large eQTL meta-analysis reveals differing patterns between cerebral cortical and cerebellar brain regions. Sci. Data *7*, 340. https://doi.org/10.1038/s41597-020-00642-8.

60. Võsa, U., Claringbould, A., Westra, H.-J., Bonder, M.J., Deelen, P., Zeng, B., Kirsten, H., Saha, A., Kreuzhuber, R., Yazar, S., et al. (2021). Large-scale cis- and trans-eQTL analyses identify thousands of genetic loci

and polygenic scores that regulate blood gene expression. Nat. Genet. *53*, 1300–1310. https://doi.org/10.1038/s41588-021-00913-z.

61. Straub, J., Venigalla, S., and Newman, J.J. (2020). Mediator's kinase module: a modular regulator of cell fate. Stem Cells Dev. *29*, 1535–1551. https://doi.org/10.1089/scd.2020.0164.

62. Galbraith, M.D., Allen, M.A., Bensard, C.L., Wang, X., Schwinn, M.K., Qin, B., Long, H.W., Daniels, D.L., Hahn, W.C., Dowell, R.D., and Espinosa, J.M. (2013). HIF1A employs CDK8-mediator to stimulate RNAPII elongation in response to hypoxia. Cell *153*, 1327–1339. https://doi.org/10.1016/j.cell.2013.04.048.

63. Janody, F., Martirosyan, Z., Benlali, A., and Treisman, J.E. (2003). Two subunits of the Drosophila mediator complex act together to control cell affinity. Development *130*, 3691–3701. https://doi.org/10.1242/dev.00607.

64. Burroughs, A.M., Iyer, L.M., and Aravind, L. (2013). Two novel PIWI families: roles in inter-genomic conflicts in bacteria and Mediator-dependent modulation of transcription in eukaryotes. Biol. Direct *8*, 13. https://doi.org/10.1186/1745-6150-8-13.

65. Galbraith, M.D., Andrysik, Z., Pandey, A., Hoh, M., Bonner, E.A., Hill, A.A., Sullivan, K.D., and Espinosa, J.M. (2017). CDK8 kinase activity promotes glycolysis. Cell Rep. *21*, 1495–1506. https://doi.org/10.1016/j.celrep.2017.10.058.

66. Lunt, S.Y., and Vander Heiden, M.G. (2011). Aerobic glycolysis: meeting the metabolic requirements of cell proliferation. Annu. Rev. Cell Dev. Biol. *27*, 441–464. https://doi.org/10.1146/annurev-cellbio-092910-154237.

67. Legan, S.K., Rebrin, I., Mockett, R.J., Radyuk, S.N., Klichko, V.I., Sohal, R.S., and Orr, W.C. (2008). Overexpression of glucose-6-phosphate dehydrogenase extends the life span of Drosophila melanogaster. J. Biol. Chem. *283*, 32492–32499. https://doi.org/10.1074/jbc.M805832200.

68. Cai, R., Zhang, Y., Simmering, J.E., Schultz, J.L., Li, Y., Fernandez-Carasa, I., Consiglio, A., Raya, A., Polgreen, P.M., Narayanan, N.S., et al. (2019). Enhancing glycolysis attenuates Parkinson's disease progression in models and clinical databases. J. Clin. Invest. *129*, 4539–4549. https://doi.org/10.1172/JCI129987.

69. Hauser, D.N., Mamais, A., Conti, M.M., Primiani, C.T., Kumaran, R., Dillman, A.A., Langston, R.G., Beilina, A., Garcia, J.H., Diaz-Ruiz, A., et al. (2017). Hexokinases link DJ-1 to the PINK1/parkin pathway. Mol. Neurodegener. *12*, 70. https://doi.org/10.1186/s13024-017-0212-x.

70. San Martín, A., Ceballo, S., Ruminot, I., Lerchundi, R., Frommer, W.B., and Barros, L.F. (2013). A genetically encoded FRET lactate sensor and its use to detect the Warburg effect in single cancer cells. PLoS One *8*, e57712. https://doi.org/10.1371/journal.pone.0057712.

71. Donner, A.J., Szostek, S., Hoover, J.M., and Espinosa, J.M. (2007). CDK8 is a stimulus-specific positive coregulator of p53 target genes. Mol. Cell *27*, 121–133. https://doi.org/10.1016/j.molcel.2007.05.026.

72. Kato, K., Awasaki, T., and Ito, K. (2009). Neuronal programmed cell death induces glial cell division in the adult Drosophila brain. Development *136*, 51–59. https://doi.org/10.1242/dev.023366.

73. Grassi, D., Howard, S., Zhou, M., Diaz-Perez, N., Urban, N.T., Guerrero-Given, D., Kamasawa, N., Volpicelli-Daley, L.A., LoGrasso, P., and Lasmézas, C.I. (2018). Identification of a highly neurotoxic α-synuclein species inducing mitochondrial damage and mitophagy in Parkinson's disease. Proc. Natl. Acad. Sci. USA *115*, E2634–E2643. https://doi.org/10.1073/pnas.1713849115.

74. Albrecht, S.C., Barata, A.G., Grosshans, J., Teleman, A.A., and Dick, T.P. (2011). In vivo mapping of hydrogen peroxide and oxidized glutathione reveals chemical and regional specificity of redox homeostasis. Cell Metab. *14*, 819–829. https://doi.org/10.1016/j.cmet.2011.10.010.

75. Tsuyama, T., Kishikawa, J.-I., Han, Y.-W., Harada, Y., Tsubouchi, A., Noji, H., Kakizuka, A., Yokoyama, K., Uemura, T., and Imamura, H. (2013). In vivo fluorescent adenosine 5'-triphosphate (ATP) imaging of Drosophila melanogaster and Caenorhabditis elegans by using a genetically encoded fluorescent ATP biosensor optimized for low temperatures. Anal. Chem. *85*, 7889–7896. https://doi.org/10.1021/ac4015325.

76. Rangaraju, V., Calloway, N., and Ryan, T.A. (2014). Activity-driven local ATP synthesis is required for synaptic function. Cell *156*, 825–835. https://doi.org/10.1016/j.cell.2013.12.042.

77. Guo, F., Yu, J., Jung, H.J., Abruzzi, K.C., Luo, W., Griffith, L.C., and Rosbash, M. (2016). Circadian neuron feedback controls the Drosophila sleep–activity profile. Nature *536*, 292–297. https://doi.org/10.1038/nature19097.

78. Schmidt, M.M., and Dringen, R. (2012). Glutathione (GSH) synthesis and metabolism. In Neural Metabolism in Vivo, I.-Y. Choi and R. Gruetter, eds. (Springer US), pp. 1029–1050. https://doi.org/10.1007/978-1-4614-1788-0_36.

79. Lu, S.C. (2013). Glutathione synthesis. Biochim. Biophys. Acta *1830*, 3143–3153. https://doi.org/10.1016/j.bbagen.2012.09.008.

80. Gao, H., Chen, Y., and Leary, J.A. (2005). Kinetic measurements of phosphoglucose isomerase and phosphomannose isomerase by direct analysis of phosphorylated aldose–ketose isomers using tandem mass spectrometry. Int. J. Mass Spectrom. *240*, 291–299. https://doi.org/10.1016/j.ijms.2004.09.017.

81. Semenza, G.L. (2019). Pharmacologic targeting of hypoxia-inducible factors. Annu. Rev. Pharmacol. Toxicol. *59*, 379–403. https://doi.org/10.1146/annurev-pharmtox-010818-021637.

82. Bacon, N.C., Wappner, P., O'Rourke, J.F., Bartlett, S.M., Shilo, B., Pugh, C.W., and Ratcliffe, P.J. (1998). Regulation of the Drosophila bHLH-PAS protein Sima by hypoxia: functional evidence for homology with mammalian HIF-1 alpha. Biochem. Biophys. Res. Commun. *249*, 811–816. https://doi.org/10.1006/bbrc.1998.9234.

83. Giasson, B.I., Duda, J.E., Quinn, S.M., Zhang, B., Trojanowski, J.Q., and Lee, V.M.-Y. (2002). Neuronal alpha-synucleinopathy with severe movement disorder in mice expressing A53T human alpha-synuclein. Neuron *34*, 521–533. https://doi.org/10.1016/s0896-6273(02)00682-7.

84. Li, Y.I., Wong, G., Humphrey, J., and Raj, T. (2019). Prioritizing Parkinson's disease genes using population-scale transcriptomic data. Nat. Commun. *10*, 994. https://doi.org/10.1038/s41467-019-08912-9.

85. Höllerhage, M., Bickle, M., and Höglinger, G.U. (2019). Unbiased screens for modifiers of alpha-synuclein toxicity. Curr. Neurol. Neurosci. Rep. *19*, 8. https://doi.org/10.1007/s11910-019-0925-z.

86. Butler, E.K., Voigt, A., Lutz, A.K., Toegel, J.P., Gerhardt, E., Karsten, P., Falkenburger, B., Reinartz, A., Winklhofer, K.F., and Schulz, J.B. (2012). The mitochondrial chaperone protein TRAP1 mitigates alpha-synuclein toxicity. PLoS Genet. *8*, e1002488. https://doi.org/10.1371/journal.pgen.1002488.

87. Auluck, P.K., Chan, H.Y.E., Trojanowski, J.Q., Lee, V.M.Y., and Bonini, N.M. (2002). Chaperone suppression of alpha-synuclein toxicity in a Drosophila model for Parkinson's disease. Science *295*, 865–868. https://doi.org/10.1126/science.1067389.

88. Kuwahara, T., Koyama, A., Koyama, S., Yoshina, S., Ren, C.-H., Kato, T., Mitani, S., and Iwatsubo, T. (2008). A systematic RNAi screen reveals involvement of endocytic pathway in neuronal dysfunction in α-synuclein transgenic C. elegans. Hum. Mol. Genet. *17*, 2997–3009. https://doi.org/10.1093/hmg/ddn198.

89. Rousseaux, M.W.C., Vázquez-Vélez, G.E., Al-Ramahi, I., Jeong, H.-H., Bajić, A., Revelli, J.-P., Ye, H., Phan, E.T., Deger, J.M., Perez, A.M., et al. (2018). A druggable genome screen identifies modifiers of α-synuclein levels via a tiered cross-species validation approach. J. Neurosci. *38*, 9286–9301. https://doi.org/10.1523/JNEUROSCI.0254-18.2018.

90. Trinh, K., Moore, K., Wes, P.D., Muchowski, P.J., Dey, J., Andrews, L., and Pallanck, L.J. (2008). Induction of the phase II detoxification pathway suppresses neuron loss in Drosophila models of Parkinson's disease. J. Neurosci. *28*, 465–472. https://doi.org/10.1523/JNEUROSCI.4778-07.2008.

91. Branco, J., Al-Ramahi, I., Ukani, L., Pérez, A.M., Fernandez-Funez, P., Rincón-Limas, D., and Botas, J. (2008). Comparative analysis of genetic modifiers in Drosophila points to common and distinct mechanisms of pathogenesis among polyglutamine diseases. Hum. Mol. Genet. *17*, 376–390. https://doi.org/10.1093/hmg/ddm315.

92. Snijders Blok, L., Hiatt, S.M., Bowling, K.M., Prokop, J.W., Engel, K.L., Cochran, J.N., Bebin, E.M., Bijlsma, E.K., Ruivenkamp, C.A.L., Terhal, P., et al. (2018). De novo mutations in MED13, a component of the Mediator complex, are associated with a novel neurodevelopmental disorder. Hum. Genet. *137*, 375–388. https://doi.org/10.1007/s00439-018-1887-y.

93. Zhdanov, A.V., Okkelman, I.A., Collins, F.W.J., Melgar, S., and Papkovsky, D.B. (2015). A novel effect of DMOG on cell metabolism: direct inhibition of mitochondrial function precedes HIF target gene expression. Biochim. Biophys. Acta *1847*, 1254–1266. https://doi.org/10.1016/j.bbabio.2015.06.016.

94. Liemburg-Apers, D.C., Schirris, T.J.J., Russel, F.G.M., Willems, P.H.G.M., and Koopman, W.J.H. (2015). Mitoenergetic dysfunction triggers a rapid compensatory increase in steady-state glucose flux. Biophys. J. *109*, 1372–1386. https://doi.org/10.1016/j.bpj.2015.08.002.

95. Chumarina, M., Russ, K., Azevedo, C., Heuer, A., Pihl, M., Collin, A., Frostner, E.Å., Elmer, E., Hyttel, P., Cappelletti, G., et al. (2019). Cellular alterations identified in pluripotent stem cell-derived midbrain spheroids generated from a female patient with progressive external ophthalmoplegia and parkinsonism who carries a novel variation (p.Q811R) in the POLG1 gene. Acta Neuropathol. Commun. *7*, 208. https://doi.org/10.1186/s40478-019-0863-7.

96. González-Rodríguez, P., Zampese, E., Stout, K.A., Guzman, J.N., Ilijic, E., Yang, B., Tkatch, T., Stavarache, M.A., Wokosin, D.L., Gao, L., et al. (2021). Disruption of mitochondrial complex I induces progressive parkinsonism. Nature *599*, 650–656. https://doi.org/10.1038/s41586-021-04059-0.

97. Lee, S.-J., Hwang, A.B., and Kenyon, C. (2010). Inhibition of respiration extends C. elegans life span via reactive oxygen species that increase HIF-1 activity. Curr. Biol. *20*, 2131–2136. https://doi.org/10.1016/j.cub.2010.10.057.

98. Ma, Z., Wang, H., Cai, Y., Wang, H., Niu, K., Wu, X., Ma, H., Yang, Y., Tong, W., Liu, F., et al. (2018). Epigenetic drift of H3K27me3 in aging links glycolysis to healthy longevity in Drosophila. Elife *7*, e35368. https://doi.org/10.7554/eLife.35368.

99. Oka, M., Suzuki, E., Asada, A., Saito, T., Iijima, K.M., and Ando, K. (2021). Increasing neuronal glucose uptake attenuates brain aging and promotes life span under dietary restriction in Drosophila. iScience *24*, 101979. https://doi.org/10.1016/j.isci.2020.101979.

100. Frame, A.K., Simon, A.F., and Cumming, R.C. (2020). Determining the role of lactate metabolism on age-dependent memory decline and neurodegeneration in Drosophila melanogaster. Alzheimers. Dement. *16*. https://doi.org/10.1002/alz.037313.

101. Niccoli, T., Kerr, F., Snoeren, I., Fabian, D., Aleyakpo, B., Ivanov, D., Sofola-Adesakin, O., Cryar, A., Adcott, J., Thornton, J., and Partridge, L. (2021). Activating transcription factor 4-dependent lactate dehydrogenase activation as a protective response to amyloid beta toxicity. Brain Commun. *3*, fcab053. https://doi.org/10.1093/braincomms/fcab053.

102. Beebe, K., Robins, M.M., Hernandez, E.J., Lam, G., Horner, M.A., and Thummel, C.S. (2020). Drosophila estrogen-related receptor directs a transcriptional switch that supports adult glycolysis and lipogenesis. Genes Dev. *34*, 701–714. https://doi.org/10.1101/gad.335281.119.

103. Homem, C.C.F., Steinmann, V., Burkard, T.R., Jais, A., Esterbauer, H., and Knoblich, J.A. (2014). Ecdysone and mediator change energy metabolism to terminate proliferation in Drosophila neural stem cells. Cell *158*, 874–888. https://doi.org/10.1016/j.cell.2014.06.024.

104. Patten, D.A., McGuirk, S., Anilkumar, U., Antoun, G., Gandhi, K., Parmar, G., Iqbal, M.A., Wong, J., Richardson, R.B., St-Pierre, J., et al. (2021). Altered mitochondrial fusion drives defensive glutathione synthesis in cells able to switch to glycolytic ATP production. Biochim. Biophys. Acta. Mol. Cell Res. *1868*, 118854. https://doi.org/10.1016/j.bbamcr.2020.118854.

105. Liu, C., and Yu, J. (2019). Genome-wide association studies for cerebrospinal fluid soluble TREM2 in Alzheimer's disease. Front. Aging Neurosci. *11*, 297. https://doi.org/10.3389/fnagi.2019.00297.

106. Kunkle, B.W., Grenier-Boley, B., Sims, R., Bis, J.C., Damotte, V., Naj, A.C., Boland, A., Vronskaya, M., van der Lee, S.J., Amlie-Wolf, A., et al. (2019). Genetic meta-analysis of diagnosed Alzheimer's disease identifies new risk loci and implicates Aβ, tau, immunity and lipid processing. Nat. Genet. *51*, 414–430. https://doi.org/10.1038/s41588-019-0358-2.

107. Chibnik, L.B., White, C.C., Mukherjee, S., Raj, T., Yu, L., Larson, E.B., Montine, T.J., Keene, C.D., Sonnen, J., Schneider, J.A., et al. (2018). Susceptibility to neurofibrillary tangles: role of the PTPRD locus and limited pleiotropy with other neuropathologies. Mol. Psychiatry *23*, 1521–1529. https://doi.org/10.1038/mp.2017.20.

108. Wang, H., Yang, J., Schneider, J.A., De Jager, P.L., Bennett, D.A., and Zhang, H.-Y. (2020). Genome-wide interaction analysis of pathological hallmarks in Alzheimer's disease. Neurobiol. Aging *93*, 61–68. https://doi.org/10.1016/j.neurobiolaging.2020.04.025.

109. Qin, L., Shu, L., Zhong, J., Pan, H., Guo, J., Sun, Q., Yan, X., Tang, B., and Xu, Q. (2019). Association of HIF1A and Parkinson's disease in a Han Chinese population demonstrated by molecular inversion probe analysis. Neurol. Sci. *40*, 1927–1931. https://doi.org/10.1007/s10072-019-03905-4.

110. Zaman, K., Ryu, H., Hall, D., O'Donovan, K., Lin, K.I., Miller, M.P., Marquis, J.C., Baraban, J.M., Semenza, G.L., and Ratan, R.R. (1999). Protection from oxidative stress-induced apoptosis in cortical neuronal cultures by iron chelators is associated with enhanced DNA binding of hypoxia-inducible factor-1 and ATF-1/CREB and increased expression of glycolytic enzymes, p21(waf1/cip1), and erythropoietin. J. Neurosci. *19*, 9821–9830.

111. Febbraro, F., Andersen, K.J., Sanchez-Guajardo, V., Tentillier, N., and Romero-Ramos, M. (2013). Chronic intranasal deferoxamine ameliorates motor defects and pathology in the α-synuclein rAAV Parkinson's model. Exp. Neurol. *247*, 45–58. https://doi.org/10.1016/j.expneurol.2013.03.017.

112. During, M.J., Cao, L., Zuzga, D.S., Francis, J.S., Fitzsimons, H.L., Jiao, X., Bland, R.J., Klugmann, M., Banks, W.A., Drucker, D.J., and Haile, C.N. (2003). Glucagon-like peptide-1 receptor is involved in learning and neuroprotection. Nat. Med. *9*, 1173–1179. https://doi.org/10.1038/nm919.

113. Daniele, G., Iozzo, P., Molina-Carrion, M., Lancaster, J., Ciociaro, D., Cersosimo, E., Tripathy, D., Triplitt, C., Fox, P., Musi, N., et al. (2015). Exenatide regulates cerebral glucose metabolism in brain areas associated with glucose homeostasis and reward system. Diabetes *64*, 3406–3412. https://doi.org/10.2337/db14-1718.

114. Athauda, D., Maclagan, K., Skene, S.S., Bajwa-Joseph, M., Letchford, D., Chowdhury, K., Hibbert, S., Budnik, N., Zampedri, L., Dickson, J., et al. (2017). Exenatide once weekly versus placebo in Parkinson's disease: a randomised, double-blind, placebo-controlled trial. Lancet *390*, 1664–1675. https://doi.org/10.1016/S0140-6736(17)31585-4.

115. Mulvaney, C.A., Duarte, G.S., Handley, J., Evans, D.J., Menon, S., Wyse, R., and Emsley, H.C. (2020). GLP-1 receptor agonists for Parkinson's disease. Cochrane Database Syst. Rev. *7*, CD012990. https://doi.org/10.1002/14651858.CD012990.pub2.

116. Chen, R., Shi, L., Hakenberg, J., Naughton, B., Sklar, P., Zhang, J., Zhou, H., Tian, L., Prakash, O., Lemire, M., et al. (2016). Analysis of 589, 306 genomes identifies individuals resilient to severe Mendelian childhood diseases. Nat. Biotechnol. *34*, 531–538. https://doi.org/10.1038/nbt.3514.

117. Sheridan, C. (2019). Unicorn startup trawls databases for protective genetic modifiers. Nat. Biotechnol. *37*, 487–489. https://doi.org/10.1038/d41587-019-00010-x.

118. Su, L.J., Auluck, P.K., Outeiro, T.F., Yeger-Lotem, E., Kritzer, J.A., Tardiff, D.F., Strathearn, K.E., Liu, F., Cao, S., Hamamichi, S., et al. (2010). Compounds from an unbiased chemical screen reverse both ER-to-Golgi trafficking defects and mitochondrial dysfunction in Parkinson's disease

models. Dis. Model. Mech. *3*, 194–208. https://doi.org/10.1242/dmm.004267.

119. Li, G., and Hidalgo, A. (2020). Adult neurogenesis in the Drosophila brain: the evidence and the void. Int. J. Mol. Sci. *21*, 6653. https://doi.org/10.3390/ijms21186653.

120. Billings, J.L., Hare, D.J., Nurjono, M., Volitakis, I., Cherny, R.A., Bush, A.I., Adlard, P.A., and Finkelstein, D.I. (2016). Effects of neonatal iron feeding and chronic clioquinol administration on the parkinsonian human A53T transgenic mouse. ACS Chem. Neurosci. *7*, 360–366. https://doi.org/10.1021/acschemneuro.5b00305.

121. Finkelstein, D.I., Hare, D.J., Billings, J.L., Sedjahtera, A., Nurjono, M., Arthofer, E., George, S., Culvenor, J.G., Bush, A.I., and Adlard, P.A. (2016). Clioquinol improves cognitive, motor function, and microanatomy of the alpha-synuclein hA53T transgenic mice. ACS Chem. Neurosci. *7*, 119–129. https://doi.org/10.1021/acschemneuro.5b00253.

122. Billings, J.L., Gordon, S.L., Rawling, T., Doble, P.A., Bush, A.I., Adlard, P.A., Finkelstein, D.I., and Hare, D.J. (2019). l-3, 4-dihydroxyphenylalanine (l-DOPA) modulates brain iron, dopaminergic neurodegeneration and motor dysfunction in iron overload and mutant alpha-synuclein mouse models of Parkinson's disease. J. Neurochem. *150*, 88–106. https://doi.org/10.1111/jnc.14676.

123. Parkkinen, L., O'Sullivan, S.S., Collins, C., Petrie, A., Holton, J.L., Revesz, T., and Lees, A.J. (2011). Disentangling the relationship between Lewy bodies and nigral neuronal loss in Parkinson's disease. J. Parkinsons Dis. *1*, 277–286. https://doi.org/10.3233/JPD-2011-11046.

124. Jellinger, K.A. (2019). Is Braak staging valid for all types of Parkinson's disease? J. Neural. Transm. *126*, 423–431. https://doi.org/10.1007/s00702-018-1898-9.

125. Cingolani, P., Platts, A., Wang, L.L., Coon, M., Nguyen, T., Wang, L., Land, S.J., Lu, X., and Ruden, D.M. (2012). A program for annotating and predicting the effects of single nucleotide polymorphisms, SnpEff: SNPs in the genome of Drosophila melanogaster strain w1118 ; iso-2; iso-3. Fly *6*, 80–92.

126. McKenna, A., Hanna, M., Banks, E., Sivachenko, A., Cibulskis, K., Kernytsky, A., Garimella, K., Altshuler, D., Gabriel, S., Daly, M., and DePristo, M.A. (2010). The Genome Analysis Toolkit: a MapReduce framework for analyzing next-generation DNA sequencing data. Genome Res. *20*, 1297–1303. https://doi.org/10.1101/gr.107524.110.

127. Cingolani, P., Patel, V.M., Coon, M., Nguyen, T., Land, S.J., Ruden, D.M., and Lu, X. (2012). Using Drosophila melanogaster as a model for genotoxic chemical mutational studies with a new program. Front. Genet. *3*, 35. https://doi.org/10.3389/fgene.2012.00035.

128. dos Santos, G., Schroeder, A.J., Goodman, J.L., Strelets, V.B., Crosby, M.A., Thurmond, J., Emmert, D.B., and Gelbart, W.M.; FlyBase Consortium (2015). FlyBase: introduction of the Drosophila melanogaster Release 6 reference genome assembly and large-scale migration of genome annotations. Nucleic Acids Res. *43*, D690–D697. https://doi.org/10.1093/nar/gku1099.

129. Groth, A.C., Fish, M., Nusse, R., and Calos, M.P. (2004). Construction of transgenic Drosophila by using the site-specific integrase from phage phiC31. Genetics *166*, 1775–1782. https://doi.org/10.1534/genetics.166.4.1775.

130. Venken, K.J.T., Carlson, J.W., Schulze, K.L., Pan, H., He, Y., Spokony, R., Wan, K.H., Koriabine, M., de Jong, P.J., White, K.P., et al. (2009). Versatile P[acman] BAC libraries for transgenesis studies in Drosophila melanogaster. Nat. Methods *6*, 431–434. https://doi.org/10.1038/nmeth.1331.

131. Koh, T.W., He, Z., Gorur-Shandilya, S., Menuz, K., Larter, N.K., Stewart, S., and Carlson, J.R. (2014). The Drosophila IR20a clade of ionotropic receptors are candidate taste and pheromone receptors. Neuron *83*, 850–865. https://doi.org/10.1016/j.neuron.2014.07.012.

132. Markstein, M., Pitsouli, C., Villalta, C., Celniker, S.E., and Perrimon, N. (2008). Exploiting position effects and the gypsy retrovirus insulator to engineer precisely expressed transgenes. Nat. Genet. *40*, 476–483. https://doi.org/10.1038/ng.101.

133. Chouhan, A.K., Guo, C., Hsieh, Y.-C., Ye, H., Senturk, M., Zuo, Z., Li, Y., Chatterjee, S., Botas, J., Jackson, G.R., et al. (2016). Uncoupling neuronal death and dysfunction in Drosophila models of neurodegenerative disease. Acta Neuropathol. Commun. *4*, 62. https://doi.org/10.1186/s40478-016-0333-4.

134. Wang, C.-T., Chen, Y.-C., Wang, Y.-Y., Huang, M.-H., Yen, T.-L., Li, H., Liang, C.-J., Sang, T.-K., Ciou, S.-C., Yuh, C.-H., et al. (2012). Reduced neuronal expression of ribose-5-phosphate isomerase enhances tolerance to oxidative stress, extends lifespan, and attenuates polyglutamine toxicity in Drosophila. Aging Cell *11*, 93–103. https://doi.org/10.1111/j.1474-9726.2011.00762.x.

135. Xu, T., and Rubin, G.M. (1993). Analysis of genetic mosaics in developing and adult Drosophila tissues. Development *117*, 1223–1237.

136. Riemensperger, T., Issa, A.-R., Pech, U., Coulom, H., Nguyễn, M.-V., Cassar, M., Jacquet, M., Fiala, A., and Birman, S. (2013). A single dopamine pathway underlies progressive locomotor deficits in a Drosophila model of Parkinson disease. Cell Rep. *5*, 952–960. https://doi.org/10.1016/j.celrep.2013.10.032.

137. Verstreken, P., Ly, C.V., Venken, K.J.T., Koh, T.-W., Zhou, Y., and Bellen, H.J. (2005). Synaptic mitochondria are critical for mobilization of reserve pool vesicles at Drosophila neuromuscular junctions. Neuron *47*, 365–378. https://doi.org/10.1016/j.neuron.2005.06.018.

138. Schindelin, J., Arganda-Carreras, I., Frise, E., Kaynig, V., Longair, M., Pietzsch, T., Preibisch, S., Rueden, C., Saalfeld, S., Schmid, B., et al. (2012). Fiji: an open-source platform for biological-image analysis. Nat. Methods *9*, 676–682. https://doi.org/10.1038/nmeth.2019.

139. Sunderhaus, E.R., and Kretzschmar, D. (2016). Mass histology to quantify neurodegeneration in Drosophila. J. Vis. Exp., e54809. https://doi.org/10.3791/54809.

140. Haelterman, N.A., Jiang, L., Li, Y., Bayat, V., Sandoval, H., Ugur, B., Tan, K.L., Zhang, K., Bei, D., Xiong, B., et al. (2014). Large-scale identification of chemically induced mutations in Drosophila melanogaster. Genome Res. *24*, 1707–1718. https://doi.org/10.1101/gr.174615.114.

141. Khalfan, M. (2016). Variant Calling Pipeline: FastQ to Annotated SNPs in Hours. https://gencore.bio.nyu.edu/variant-calling-pipeline/.

142. Auwera, G.A., Carneiro, M.O., Hartl, C., Poplin, R., Del Angel, G., Levy-Moonshine, A., Jordan, T., Shakir, K., Roazen, D., Thibault, J., et al. (2013). From FastQ data to high confidence variant calls: the Genome Analysis Toolkit best practices pipeline. Curr. Protoc. Bioinformatics *43*, 11. https://doi.org/10.1002/0471250953.bi1110s43.

143. Wang, F., Jiang, L., Chen, Y., Haelterman, N.A., Bellen, H.J., and Chen, R. (2015). FlyVar: a database for genetic variation in Drosophila melanogaster. Database *2015*, bav079. https://doi.org/10.1093/database/bav079.

144. Mackay, T.F.C., Richards, S., Stone, E.A., Barbadilla, A., Ayroles, J.F., Zhu, D., Casillas, S., Han, Y., Magwire, M.M., Cridland, J.M., et al. (2012). The Drosophila melanogaster genetic reference panel. Nature *482*, 173–178. https://doi.org/10.1038/nature10811.

145. Potter, C.J., Tasic, B., Russler, E.V., Liang, L., and Luo, L. (2010). The Q system: a repressible binary system for transgene expression, lineage tracing, and mosaic analysis. Cell *141*, 536–548. https://doi.org/10.1016/j.cell.2010.02.025.

146. McGuire, S.E., Mao, Z., and Davis, R.L. (2004). Spatiotemporal gene expression targeting with the TARGET and gene-switch systems in Drosophila. Sci. STKE, l6. https://doi.org/10.1126/stke.2202004pl6.

147. Bertolin, A.P., Katz, M.J., Yano, M., Pozzi, B., Acevedo, J.M., Blanco-Obregón, D., Gándara, L., Sorianello, E., Kanda, H., Okano, H., et al. (2016). Musashi mediates translational repression of the Drosophila hypoxia inducible factor. Nucleic Acids Res. *44*, 7555–7567. https://doi.org/10.1093/nar/gkw372.

148. Llamazares, S., Moreira, A., Tavares, A., Girdham, C., Spruce, B.A., Gonzalez, C., Karess, R.E., Glover, D.M., and Sunkel, C.E. (1991). Polo

encodes a protein kinase homolog required for mitosis in Drosophila. Genes Dev. *5*, 2153–2165. https://doi.org/10.1101/gad.5.12a.2153.

149. Kachaner, D., Garrido, D., Mehsen, H., Normandin, K., Lavoie, H., and Archambault, V. (2017). Coupling of Polo kinase activation to nuclear localization by a bifunctional NLS is required during mitotic entry. Nat. Commun. *8*, 1701. https://doi.org/10.1038/s41467-017-01876-8.

150. Skeath, J.B., Wilson, B.A., Romero, S.E., Snee, M.J., Zhu, Y., and Lacin, H. (2017). The extracellular metalloprotease AdamTS-A anchors neural lineages in place within and preserves the architecture of the central nervous system. Development *144*, 3102–3113. https://doi.org/10.1242/dev.145854.

151. Gutscher, M., Pauleau, A.-L., Marty, L., Brach, T., Wabnitz, G.H., Samstag, Y., Meyer, A.J., and Dick, T.P. (2008). Real-time imaging of the intracellular glutathione redox potential. Nat. Methods *5*, 553–559. https://doi.org/10.1038/nmeth.1212.

152. Gutscher, M., Sobotta, M.C., Wabnitz, G.H., Ballikaya, S., Meyer, A.J., Samstag, Y., and Dick, T.P. (2009). Proximity-based protein thiol oxidation by H2O2-scavenging peroxidases. J. Biol. Chem. *284*, 31532–31540. https://doi.org/10.1074/jbc.M109.059246.

153. Olsen, A.L., and Feany, M.B. (2019). Glial α-synuclein promotes neurodegeneration characterized by a distinct transcriptional program in vivo. Glia *67*, 1933–1957. https://doi.org/10.1002/glia.23671.

154. Taylor, S.C., Nadeau, K., Abbasi, M., Lachance, C., Nguyen, M., and Fenrich, J. (2019). The ultimate qPCR experiment: producing publication quality, reproducible data the first time. Trends Biotechnol. *37*, 761–774. https://doi.org/10.1016/j.tibtech.2018.12.002.

155. Lee, B.R., and Kamitani, T. (2011). Improved immunodetection of endogenous α-synuclein. PLoS One *6*, e23939. https://doi.org/10.1371/journal.pone.0023939.

156. Ghanem, S.S., Majbour, N.K., Vaikath, N.N., Ardah, M.T., Erskine, D., Jensen, N.M., Fayyad, M., Sudhakaran, I.P., Vasili, E., Melachroinou, K., et al. (2022). α-Synuclein phosphorylation at serine 129 occurs after initial protein deposition and inhibits seeded fibril formation and toxicity. Proc. Natl. Acad. Sci. USA *119*, e2109617119. https://doi.org/10.1073/pnas.2109617119.

157. Elfarrash, S., Jensen, N.M., Ferreira, N., Schmidt, S.I., Gregersen, E., Vestergaard, M.V., Nabavi, S., Meyer, M., and Jensen, P.H. (2021). Polo-like kinase 2 inhibition reduces serine-129 phosphorylation of physiological nuclear alpha-synuclein but not of the aggregated alpha-synuclein. PLoS One *16*, e0252635. https://doi.org/10.1371/journal.pone.0252635.

158. Ip, C.W., Cheong, D., and Volkmann, J. (2017). Stereological estimation of dopaminergic neuron number in the mouse substantia nigra using the optical fractionator and standard microscopy equipment. J. Vis. Exp. *127*, e56103. https://doi.org/10.3791/56103.

159. Joshi, A.U., Minhas, P.S., Liddelow, S.A., Haileselassie, B., Andreasson, K.I., Dorn, G.W., 2nd, and Mochly-Rosen, D. (2019). Fragmented mitochondria released from microglia trigger A1 astrocytic response and propagate inflammatory neurodegeneration. Nat. Neurosci. *22*, 1635–1648. https://doi.org/10.1038/s41593-019-0486-0.

160. Valente, A.J., Maddalena, L.A., Robb, E.L., Moradi, F., and Stuart, J.A. (2017). A simple ImageJ macro tool for analyzing mitochondrial network morphology in mammalian cell culture. Acta Histochem. *119*, 315–326. https://doi.org/10.1016/j.acthis.2017.03.001.

STAR★METHODS

KEY RESOURCES TABLE

REAGENT or RESOURCE	SOURCE	IDENTIFIER
Antibodies		
Chicken anti-SNCA	Abcam	ab190376
Rabbit anti-α-synuclein	Abcam	ab155038
Mouse anti-α-synuclein (clone 42)	BD Biosciences	AB_398107
Rabbit anti-α-synuclein (clone MJFR1)	Abcam	ab138501
Rabbit phospho-α-synuclein (Ser 129, clone D1R1R)	Cell Signaling Technology	23706
Rabbit anti-Gpi	Merck	HPA024305
Rabbit anti-Pgk2	Merck	HPA073656
Rabbit anti-LDH	Aviva Systems Biology	OAAB06120
Rabbit anti-PH3(Ser10)	Millipore	06–570
Mouse anti-PCNA (PC10)	Thermo Fisher Scientific	13–3900
Mouse anti-Polo kinase (clone MA294)	Laboratory of David Glover	MA294
Guinea pig anti-Deadpan (Dpn)	Skeath et al.[125] (via Yu Cai)	N/A
Mouse anti alpha-Tubulin, 12G10	DSHB	12G10
Rabbit anti-Tyrosine Hydroxylase (TH)	Pel Freeze	P40101-0
Chicken anti-Tyrosine Hydroxylase	Abcam	ab76442
Rabbit anti-Skd	Janody et al.[47]	N/A
Rabbit anti-Sima	Bertolin et al.[126]	N/A
Mouse anti-Elav (clone 9F8A9)	DSHB	9F8A9
Rat anti-Elav (clone 7E8A10)	DSHB	clone 7E8A10
Mouse anti-MED13/TRAP240	Santa Cruz Biotechnology	sc-515557
Mouse anti-beta actin	Abcam	ab8226
Rabbit anti-TOM20 (clone EPR15581-54)	Abcam	ab186735
Rabit anti-NeuN (clone EPR12763)	Abcam	ab177487
Rabbit anti-MED12	Abcam	ab70842
Rabbit anti-CDK8	Thermo Fisher Scientific	A302-501A-T
Rabbit anti-Cyclin C	Thermo Fisher Scientific	A301-989A
Rabbit anti-CRSP1/TRAP220 (MED1)	Thermo Fisher Scientific	A300-793A
Rabbit anti-MED15	Thermo Fisher Scientific	A302-422A
Bacterial and virus strains		
Adeno-associated virus strain *HBAAV2/9-EGFP NC*	HanBio, Shanghai	N/A (see Table S2 for shRNA sequences)
Adeno-associated virus strain *HBAAV2/9-m-Med13 shRNA1-EGFP*	HanBio, Shanghai	N/A (see Table S2 for shRNA sequences)
Chemicals, peptides, and recombinant proteins		
Paraplast X-TRA	Sigma-Aldrich	P3808
Methyl benzoate	Sigma-Aldrich	M29908-500G
Heat sink for Traco	RS Components	TEN-HS4
Glutaraldehyde	Electron Microscopy Sciences	16200
Paraformaldehyde	Electron Microscopy Sciences	15713
Toluidine blue	Sigma-Aldrich	T3260
Permount™ Mounting Medium	Electron Microscopy Sciences	17986–01
4′, 6-diamidino-2-phenylindole (DAPI)	Thermo Fisher Scientific	62248
ProLong™ Gold Antifade Mountant	Thermo Fisher Scientific	P36934

(*Continued on next page*)

Continued

REAGENT or RESOURCE	SOURCE	IDENTIFIER
VectaShield Mounting Medium	Vector Laboratories	H-1000
Ultramicrotome	Leica Biosystems Microtomes	Leica Ultracut UCT
Mini Protean TGX (stain-free) 4–20%	Bio-Rad	4568096
Deferoxamine mesylate salt, powder, ≥92.5% (TLC)	Sigma-Aldrich	D9533-1G
RNAlater	Thermo Fisher Scientific	AM7020
RNAzol RT	Sigma-Aldrich	R4533
dsDNase	Thermo Fisher Scientific	EN0771
RevertAid First Strand cDNA Synthesis Kit	Thermo Fisher Scientific	K1621
Maxima SYBR Green/ROX qPCR Master Mix (2X)	Thermo Fisher Scientific	K0221
O.C.T. compound	Sakura	4583
Experimental models: Organisms/strains		
D. melanogaster: *KG02776*	Bloomington *Drosophila* Stock Center (mapping kit)	Flybase: FBti0021194
D. melanogaster: *KG00023*	Bloomington *Drosophila* Stock Center (mapping kit)	Flybase: FBti0021413
D. melanogaster: *KG02042*	Bloomington *Drosophila* Stock Center (mapping kit)	Flybase: FBti0023386
D. melanogaster: *BG00690*	Bloomington *Drosophila* Stock Center (mapping kit)	Flybase: FBti0040536
D. melanogaster: *BG02493*	Bloomington *Drosophila* Stock Center (mapping kit)	Flybase: FBti0040538
D. melanogaster: *BG01780*	Bloomington *Drosophila* Stock Center (mapping kit)	Flybase: FBti0040539
D. melanogaster: *BG02270*	Bloomington *Drosophila* Stock Center (mapping kit)	Flybase: FBti0018128
D. melanogaster: *BG02748*	Bloomington *Drosophila* Stock Center (mapping kit)	Flybase: FBti0021320
D. melanogaster: *BG02734*	Bloomington *Drosophila* Stock Center (mapping kit)	Flybase: FBti0018579
D. melanogaster: *BG01881*	Bloomington *Drosophila* Stock Center (mapping kit)	Flybase: FBti0017658
D. melanogaster: *BG02475*	Bloomington *Drosophila* Stock Center (mapping kit)	Flybase: FBti0017729
D. melanogaster: *BG02628*	Bloomington *Drosophila* Stock Center (mapping kit)	Flybase: FBti0017756
D. melanogaster: *w[1118]*, isogenic Roote strain	Bloomington *Drosophila* Stock Center	RRID:BDSC_5905
D. melanogaster: *y* w*; FRT80B[iso7]/ TM6b, P[y+]*	This work, isogenized third chromosome containing *FRT80B*	N/A
D. melanogaster: *Ddc-GAL4* on chromosome 2	Bloomington *Drosophila* Stock Center	RRID:BDSC_7009
D. melanogaster: *elav-GAL4* on chromosome 2 (cytological position 42C7)	Bloomington *Drosophila* Stock Center	RRID:BDSC_8765
D. melanogaster: *P{w[+mC] = tubP-GAL80 [ts]}20* (cytological position 29B1)	Bloomington *Drosophila* Stock Center	RRID:BDSC_7019
D. melanogaster: *Rh1-Gal4* on chromosome 2	Chouhan et al.[121]	N/A
D. melanogaster: *P{w[+m*] = nSyb-GAL4.S} 3* on chromosome 3	Bloomington *Drosophila* Stock Center	RRID:BDSC_51635

(*Continued on next page*)

Continued

REAGENT or RESOURCE	SOURCE	IDENTIFIER
D. melanogaster: *P{w[+mC] = UAS-SNCA.J}7*	Chouhan et al.;[121] also available at Bloomington *Drosophila* Stock Center	RRID:BDSC_51376
D. melanogaster: *UAS-Hsap\SNCA.A30P*	Bloomington *Drosophila* Stock Center	RRID:BDSC_8147
D. melanogaster: *UAS-Hsap\SNCA.A53T*	Bloomington *Drosophila* Stock Center	Flybase: FBti0040567
D. melanogaster: *UAS-cyto-Grx1-roGFP2*	Bloomington *Drosophila* Stock Center	RRID:BDSC_67662
D. melanogaster: *Df(3L)BSC449*	Bloomington *Drosophila* Stock Center	RRID:BDSC_24953
D. melanogaster: *Df(3L)BSC553*	Bloomington *Drosophila* Stock Center	RRID:BDSC_25116
D. melanogaster: *Df(3L)BSC797*	Bloomington *Drosophila* Stock Center	RRID:BDSC_27369
D. melanogaster: *skd/Med13[T13]*	Bloomington *Drosophila* Stock Center	RRID:BDSC_63123
D. melanogaster: *skd/Med13[T413]*	Bloomington *Drosophila* Stock Center	RRID:BDSC_63124
D. melanogaster: *skd/Med13[T606]*	Janody et al.[47]	Flybase: FBal0121621
D. melanogaster: *skd/Med13[2]*	Bloomington *Drosophila* Stock Center	BDSC:5047
D. melanogaster: *skd/Med13[MI12229]*	Bloomington *Drosophila* Stock Center	BDSC:57899
D. melanogaster: *skd/Med13[rK760]*	Bloomington *Drosophila* Stock Center	BDSC:10197
D. melanogaster: *P{TKO.GS00715}attP40*, CRISPR transgene targeting *GlyRS*	Bloomington *Drosophila* Stock Center	RRID:BDSC_77199
D. melanogaster: *P{nos-Cas9.R}attP40*	Bloomington *Drosophila* Stock Center	RRID:BDSC_78781
D. melanogaster: *GlyRS[C2]*	This work. Generated from *P{TKO.GS00715}attP40*	N/A
D. melanogaster: *PBac{GlyRS gDNA} VK00037*	This work	N/A
D. melanogaster: *EGFP* RNAi	Bloomington *Drosophila* Stock Center	BDSC:41556
D. melanogaster: *QUAS-SNCA*	Ordonez et al.[14]	Flybase: FBal0337971
D. melanogaster: *nSyb-QF2*	Bloomington *Drosophila* Stock Center	Flybase: FBti0154980
D. melanogaster: *skd/Med13[HMS01305]* RNAi strain	Bloomington *Drosophila* Stock Center	BDSC:34630
D. melanogaster: *kto/Med12[HMS06027]* RNAi strain	Bloomington *Drosophila* Stock Center	BDSC:80447
D. melanogaster: *Cdk8[GL00231]* RNAi strain	Bloomington *Drosophila* Stock Center	BDSC:35324
D. melanogaster: *CycC[HMS01095]* RNAi strain	Bloomington *Drosophila* Stock Center	BDSC:33753
D. melanogaster: *UAS-Pgi* on chromosome 2	Bloomington *Drosophila* Stock Center	Flybase: FBal0256731; RRID:BDSC_60676
D. melanogaster: *UAS-G6PD* on chromosome 2	Legan et al.[51]	Flybase: FBtp0071752
D. melanogaster: *P{attP,y+,w3'}VIE-260B*	Vienna *Drosophila* Resource Center	Flybase: FBti0116272; VDRC ID: 60100
D. melanogaster: *Vhl[KK111257]*	Vienna *Drosophila* Resource Center	VDRC ID: 108920; Flybase: FBti0160185
D. melanogaster: *Hph[KK100344]*	Vienna *Drosophila* Resource Center	VDRC ID: 103382; Flybase: FBti0116422
D. melanogaster: *Sima[KK102226]*	Vienna *Drosophila* Resource Center	VDRC ID: 106187; Flybase: FBti0117325
D. melanogaster: *CH321-8J6*	This work (transgenesis by Genetivision)	Flybase: FBcl0754967
D. melanogaster: *UAS-mito-roGFP2-Orp1* on chromosome 2	Bloomington *Drosophila* Stock Center	BDSC:67667
D. melanogaster: *UAS-AT1.03NL* on chromosome 2	Tsuyama et al.[59]	FBtp0108474

(*Continued on next page*)

Continued

REAGENT or RESOURCE	SOURCE	IDENTIFIER
D. melanogaster: *UAS-cyto-Grx1-roGFP2* on chromosome 2	Bloomington *Drosophila* Stock Center	BDSC:67662
D. melanogaster: *P{UAS-LUC.D}* on chromosome 3	Bloomington *Drosophila* Stock Center	FBtp0013944
D. melanogaster: *PBac{nSyb-lexA::p65} VK00018*	Bloomington *Drosophila* Stock Center	FBti0157010
D. melanogaster: *P{LexAop-Laconic}attP40*	This work	N/A
D. melanogaster: *P{w[+mC] = UAS-Pfk.T}3*	Bloomington *Drosophila* Stock Center	RRID:BDSC_60675
D. melanogaster: *P{EPgy2}Ldh[EY07426]*	Bloomington *Drosophila* Stock Center	RRID:BDSC_16829
D. melanogaster: *P{GD13860}v24258*, *Pgi* RNAi on chromosome 3	Vienna *Drosophila* Resource Center	VDRC ID: 24258; Flybase ID: FBst0455391
D. melanogaster: *P{TRiP.HMS00039}attP2*, *Ldh* RNAi	Bloomington *Drosophila* Stock Center	RRID:BDSC_33640
M. musculus: *Prnp-SNCA*A53T*	The Jackson Laboratory via Nanjing BioMedical Research Institute	RRID:IMSR_JAX:004479
M. musculus: *C57/B6*	Nanjing BioMedical Research Institute	N/A
Software and algorithms		
flySpotter	This work (Srinivas Gorur-Shandilya)	https://github.com/sg-s/fly-spotter/
ImageJ/Fiji	ImageJ	https://imagej.net/software/fiji/
GraphPad Prism	GraphPad software	https://www.graphpad.com/prism
Imaris	Oxford Instruments	http://www.bitplane.com/imaris/imaris

RESOURCE AVAILABILITY

Lead contact

Requests for resources, reagents, and further information should be directed to the lead contact, Tong-Wey Koh (tongwey@tll.org.sg).

Materials availability

The fly strains generated in this study will be provided upon request.

Data and code availability

- All data reported in this paper will be shared by the lead contact upon request.
- The original code, FlySpotter, for quantifying *Drosophila* climbing assay has been deposited by S.G.-S. at GitHub and is publicly available at: https://github.com/sg-s/fly-spotter/
- Any additional information related to this paper will be shared by the lead contact upon request.

EXPERIMENTAL MODEL AND SUBJECT DETAILS

Fly stocks and transgenes

Fly crosses and aging experiments were performed at 25°C except where indicated differently in figure legends. In addition to genomic rescue transgenic strains obtained from stock centers, P[acman] genomic constructs *CH322-20A12*, *CH321-8J6*, *CH321-9N15* and *CH321-91A10* were ordered from BACPAC Resource Center and inserted in *attP* site *VK00037* by phiC31 transgenesis (Genetivision).[127,128] *Rh1-GAL4*; *P[UAS-SNCA.J7]* is maintained as a viable healthy stock. A recombinant chromosome containing *nSyb-QF2* and *QUAS-SNCA* is maintained over the balancer chromosome *TM6b*, *Tub-QS*, which prevents *SNCA* expression in the stock and keeps it healthy. Third chromosomes containing dominant modifiers of *SNCA* are double balanced with second chromosomes containing rescue transgenes, where possible, to reduce the chance of accumulating genetic suppressors. A *LexAop-Laconic* construct was generated by 3-way Gateway recombination of a *LexAop* promoter, the *Laconic* coding sequence and a *SV40* polyA signal into the pBGRY destination vector; the resulting construct was introduced into flies at the *attP40* site via the phiC31 method.[70,129,130] The *P{LexAop-Laconic}attP40* and *PBac{nSyb-lexA:p65}VK00018* transgenic flies were crossed together to construct chromosome with pan-neuronal expression of *Laconic*. The following fly stocks were kindly donated by individual investigators: the original *FRT80B* strain, Hugo Bellen; *Rh1-GAL4* and *P[UAS-SNCA.J7]*, Josh Shulman; $Med13^{T606}$, Jessica Treisman;

QUAS-SNCA, Mel Feany; *UAS-G6pd*, Horng-Dar Wang.[14,63,67,131,132] Other fly stocks were obtained from Bloomington *Drosophila* Stock Center, Vienna *Drosophila* Stock Center and Kyoto Stock Center.

Mouse model

All experiments involving mice were performed in accordance with Chinese Laboratory animal Guideline for ethical review of animal welfare (2020/05) for the care of laboratory animals. *Prnp-SNCA*A53T* transgenic mice (RRID:IMSR_JAX:004479),[83] which overexpress human A53T mutant α-syn under the control of the *prion protein* (*PRNP*) promoter, were purchased from Jackson laboratory through Nanjing BioMedical Research Institute of Nanjing University (Nanjing, China). The *Prnp-SNCA*A53T* transgenic mice (Tg) and C57/B6 control mice (non-Tg) were reared at Beijing University Health Science Center in a specific pathogen-free standard environment with a 12-h light-dark cycle with free access to food and water until sacrificing. Only male mice were used in our experiments. For the characterization of Tg and non-Tg mice in Figures 6 and S6, mice were sacrificed at 3, 6 and 18 months old. For the *MED13* knockdown experiment in Figures 7 and S7, Tg and non-Tg mice were injected with viral vectors when they were 5 months old and were sacrificed when they were 6.5 months old (see STAR Methods section "Stereotaxic injection of adeno-associated virus (AAV) with short-hairpin RNA (shRNA) and TH-positive cell counting").

METHOD DETAILS

Genetic screen for *SNCA* dominant modifier in *Drosophila*

This dominant modifier screen is based on the hypothesis that *SNCA*-associated neurodegeneration can be modulated by heterozygous mutations that do not by themselves cause neurodegeneration. In a natural population, these hypothetical modifier alleles are likely to persist as relatively common variants in heterozygous states and may not lead to disease. We further posited that many modifier alleles affect highly conserved biological processes due to the conserved nature of neuronal function[40]; hence, such modifiers are likely to confer lethal phenotypes when present in the homozygous state.

Drosophila *chemical mutagenesis*

An isogenized viable third chromosome strain carrying *P{neoFRT}80B*,[133] named *Iso7*, was subjected to ethyl methanesulfonate (EMS) mutagenesis. Males that were starved on 1% agarose for 24 h were placed on filter paper soaked in 1% sucrose solution with 1.2 mM EMS overnight. The EMS-fed males were then mated with *y w*; *hs-hid*, *Dr/TM6b*, *P[y+]* virgin females over standard fly food. The F1 larvae were heatshocked to retain only those containing the mutagenized chromosome and the *TM6b*, *P[y+]* balancer chromosome. Each single balanced F1 male was then crossed to *y w*; *hs-hid*, *Dr/TM6b*, *P[y+]* virgin females to establish a mutagenized strain. In the F3 generation, strains were checked and only the recessive lethal mutant chromosomes were retained. This mutagenesis process was conducted in 14 batches to avoid systematic bias and a total of 3471 lethal mutant strains were established. The average percentage of lethal strains across batches was 28.9% (SEM = 2.6%).

Drosophila *locomotor assay*

Two iterations of locomotor assay were performed with males that were aged for 21 days after eclosion. In each round, we used different transgenes to avoid the possibility that the genetic background of the transgenic chromosomes biasing the screen results. In the first iteration, *w*; *P[UAS-SNCA.J]4*/+; *Ddc-GAL4/Iso7* was used as the control to compare with strains carrying one copy of the mutant chromosome (*mut*), *w*; *P[UAS-SNCA.J]4*/+; *Ddc-GAL4/mut*. Here, *Ddc-GAL4* drives the expression of wildtype *SNCA* in a subset of dopaminergic neurons that includes the protocerebral anterior medial (PAM) cluster which is required for startle-induced climbing.[134] From the first iteration, 281 mutant strains that significantly enhanced the locomotor decline were retained for testing in the second iteration. In the second iteration, *w*; *elav-GAL4*/+; *UAS-SNCA.A30P/Iso7* was used as the control to compare with *w*; *elav-GAL4*/+; *UAS-SNCA.A30P/mut*; mutant strains which showed more locomotor decline than control were selected. The *elav-GAL4* transgene drives the expression of *SNCA* with a A30P pathogenic mutation in all differentiated neurons. Forty-one strains were selected to be screened for degeneration of brain morphology (see Spurr's resin embedding and semi-thin sectioning and Paraffin embedding and sectioning).

Flies of genotypes to be tested were collected with 12 flies per vial and 8 vials per group after eclosion and maintained at 25°C with food replaced twice a week. The locomotion we measured was startled-induced climbing. Each vial of flies was transferred to a 50 mL glass cylinder and tapped to the bottom. After 5 s, the climbing image was photographed using a Nikon digital single-lens reflex camera mounted on a tripod. To facilitate computational image analysis (see Quantification and statistical analysis), the following measures were taken: (1) all light sources were based on white LEDs to avoid light flicker due to alternating currents, (2) 50 mL glass cylinder (220 × 25 mm) with no markings were used (Monotaro, 33440854), (3) white styrofoam reflectors surrounded three sides of the cylinder, (4) white LED strips pointing at the reflectors lit the cylinder without shadows and reflections that could be mistaken by the algorithm as a fly, (5) the top and bottom of the glass cylinder was positioned at the top and bottom of the frame.

Spurr's resin embedding and sectioning of fly retina

Sectioning of the retina was performed as a screen for the 41 mutant strains from the second round of locomotor screen. Fourteen-day-old flies of the following genotypes were compared for the % vacuole area in either retina or lamina:

1. Rh1-GAL4/+; +/Iso7
2. Rh1-GAL4/+; +/mut

3. Rh1-GAL4/+; UAS-SNCA/Iso7
4. Rh1-GAL4/+; UAS-SNCA/mut

Selected mutants were the ones for which (4) had significantly greater % vacuole area than (3), while (1) and (2) were similar to each other.

Spurr's resin embedding and sectioning was performed with modifications from a published protocol.[135] Fly heads were cut open in one eye while submerged in fixative (PBS with 2.5% glutaraldehyde and 2% paraformaldehyde) and fixed for 4 h in a degassed container. After washing in PBS, heads were fixed in 1% osmium tetroxide in PBS for 4 h, washed in PBS and dehydrated in an ethanol series. Heads were infiltrated with a propylene oxide-Spurr's resin series and then embedded in Spurr's resin at 60°C for 48 h. For visualization under light microscopy, eyes were sectioned on an ultramicrotome (Leica Ultracut UCT) using a glass blade at a thickness of 600 nm. Toluidine blue-stained sections were imaged using a wide field microscope (ZeissAxio Observer 7). Vacuole area as a percentage of retina area was quantified using ImageJ/Fiji[136] and plotted using GraphPad Prism (GraphPad Software Inc.). For visualization under transmission electron microscopy, a Diatome diamond knife was used to cut ultrathin sections which were stained with 2% uranyl acetate and lead citrate. The sections were then visualized with a transmission electron microscope (JEM-1230; JEOL).

Paraffin embedding and sectioning of fly retina and lamina

Paraffin embedding and sectioning were performed using a published protocol.[137] Genotypes of flies were as described for Spurr's resin embedding and sectioning; we noted that results from male and female flies were qualitatively similar.

For paraffin embedding, 20 flies were anesthetized then threaded into collars consisting of two parallel stainless steel razor blades clamped onto a small heat sink (RS Components, TEN-HS4) with binder clips. Collars were submerged in Carnoy's solution (60% ethanol, 30% chloroform, 10% glacial acetic acid) for 2–4 h for fixation. Collars were then submerged in 99% ethanol for 10 min, in 100% ethanol for 10 min, then rinsed briefly in methyl benzoate before incubating in methyl benzoate at 65°C for 30 min. Collars were submerged in a tray of molten 1:1 mixture of paraffin and methyl benzoate at 65°C for 30 min, in molten paraffin at 65°C for 30 min, then in another tray of molten paraffin at 65°C for 30 min. The three trays of paraffin were reused. Finally, collars were transferred into silicone molds, tilting the collars during transfer to prevent trapping of air bubbles, then left to cool and harden overnight at room temperature.

The binder clips were removed to separate the paraffin block with fly heads, leaving the bodies in the collar. Paraffin blocks were trimmed under the microscope to leave a small row with the embedded heads, then cut into 8 μm slices using a microtome (Leica microtome, 2135 and 2165), using Leica high-profile 818 microtome blades (Leica, 14035838926). Each paraffin ribbon was transferred using forceps to room temperature water and stuck to a glass slide, then allowed to expand by dipping in a 34°C water bath for 1 - 2 s. Glass slides were allowed to dry overnight at room temperature, submerged in Histo-Clear for 1 h, then allowed to dry overnight at room temperature. Permount Mounting Medium (Electron Microscopy Sciences, 17986-01) was used to mount slides, then allowed to dry for at least 3 days.

Sections were imaged in the Cy3 channel to visualize tissue autofluorescence using either a wide-field microscope (Zeiss Axio Observer 7) or a confocal microscope (Olympus FV3000) and analyzed using Fiji/ImageJ. Experimenters were blinded to the genotypes of the samples to avoid bias.

Genetic mapping of SNCA *modifiers using lethality as a phenotype*

We employed a combination of genetic methods and DNA sequencing to identify the mutations associated with the *SNCA* modifiers. First, the approximate chromosomal location of the *SNCA* modifier-associated lethal mutations were mapped by determining meiotic recombination frequencies between the mutations and *P* element insertions from the chromosome three mapping kit.[41] Second, chromosomal deletion strains (or deficiencies) spanning the approximate location of each *SNCA* modifier were tested for non-complementation against the mutation[42]; in this step, the overlapping nature of the deficiencies were used to identify the smallest candidate interval in which each *SNCA* modifier was located. Third, lethal mutations in known genes with the interval identified using deficiencies were used to test for non-complementation against the *SNCA* modifier. Fourth, transgenic genomic constructs which include the region containing each *SNCA* modifier mutation were tested for their abilities to rescue the lethality associated with each mutation. An example of this workflow is illustrated in Figure S2 for $skd/Med13^{06-056}$.

Some of the modifier mutant chromosomes carry single lethal mutations, while some carry multiple lethal mutations. When the lethal phenotype of a homozygous modifier mutant could be rescued by a gDNA rescue transgene containing a wildtype copy of the modifier gene (Table S2), it means this modifier mutant chromosome carries only a single lethal mutation in the identified gene. Examples are $Cdc27^{02-055}$, $ABCB7^{03-232}$, $skd/Med13^{06056}$, $CG4553^{06-125}$, and cpo^{10-129}.

In cases where the lethality of the homozygous modifier mutant could not be rescued but the original modifier mutation placed in a transheterozygous combination with a second allele of the said modifier gene could be rescued by the corresponding gDNA transgene, this means that there are additional lethal mutations on the chromosome. Examples are dlt^{05-188}, $MTA1\text{-}like^{06-040}$, hdc^{06-232}, $GlyRS^{08-107}$, $l(3)87Df/Cox20^{10-122}$ and $ND\text{-}39^{11-101}$. $Eip75b^{12-111}$ is a large gene and we could not find a gDNA transgene that carries the complete sequence of this gene; hence, we did not perform a rescue.

Identification of molecular lesions

The molecular lesions associated with each *SNCA* modifier were identified using either Sanger DNA sequencing of targeted regions or whole genome sequencing using High-Throughput Sequencing (HTS). HTS data were analyzed using published methods with

modifications.[138,139] As explained previously, chemical mutagenesis introduces multiple nucleotide variants across chromosomes, but not all variants would lead to functional disruption[138]; hence, the following bioinformatic analysis helped to identify the strong candidates for functionally disruptive mutations for further confirmation. In brief, NGS data for mutant fly strains were compared to data from the *Iso7* parental strain. Variant calling was performed using the Genome Analysis Toolkit (GATK-4.0.11.0)[140,141] and the *dm6* reference genome was obtained from National Center for Biotechnology Information.[126] SnpEFF (snpEFF 4.3T) was used to both annotate (using database BDGP6.86) and predict the effects of identified variants.[142] Annotated variants were further processed using SnpSift and all variants were filtered for quality (quality score $\geq$40).[125] Variants identified in mutant strains were dropped if they were also present in the *Iso7* parental strain. Only variants present on chromosome 3 were extracted for further processing. In order to reduce noise from spontaneous and irrelevant variants, we further dropped variants that appeared in genes which were (1) found in a list of ''disposable genes'' obtained from the FlyVar database and (2) found in the *Drosophila melanogaster* Genetic Reference Panel.[143,144] The plausible location of the causal variant for each mutant strain was supplied as a window of chromosome coordinates as determined by meiotic mapping. Variants within these windows were selected for further validation with priority given to those that were designated to have a ''HIGH'' impact by SnpEff. The following list of softwares were also used: Picard 2.18.20, bedtools-2.27.1, bwa-0.7.17, samtools-1.9, R-3.5.1.

Genetic rescue of the neurodegeneration phenotype of the SNCA *modifier alleles*

To determine whether perturbation of a single gene affect *SNCA*-associated neurodegeneration, we have performed genetic rescue of the neurodegeneration phenotype for $Cdc27^{02-055}$, $ABCB7^{03-232}$, dlt^{05-188}, $CG4553^{06-125}$, $l(3)87Df/Cox20^{10-122}$ and cpo^{10-129}; in these cases, the successful rescue with gDNA transgene carrying wildtype copy of the gene-of-interest indicates that a single gene is responsible for the phenotype. Hence, the lamina neurodegeneration phenotype ''no gDNA transgene'' genotype was compared with the ''gDNA transgene'' genotype as follows, in paraffin sections:

- ''No gDNA transgene'' genotype: *Rh1-GAL4/+*; *UAS-SNCA.WT/modifier mutation*
- ''gDNA transgene'' genotype: *Rh1-GAL4/gDNA rescue*; *UAS-SNCA.WT/modifier mutation*

For the remaining modifier alleles, we did not perform genetic rescue of the neurodegeneration phenotype due to logistic challenges, such as the lack of suitable gDNA rescue transgene or the loss of strains during COVID-19 social distancing measures.

Phenocopy of the neurodegeneration phenotype of the SNCA *modifier alleles*

In cases where we do not have genetic rescue of the neurodegeneration phenotype, we used additional alleles of the modifier gene or RNAi knockdown to phenocopy the EMS alleles we have initially isolated. Hence, EMS alleles of *dlt*, *MTA1-like*, *skd/Med13*, *CG4553*, *hdc*, *GlyRS*, *ND-39* and *Eip75B* were each verified by demonstration of the enhancement of *SNCA*-associated neurodegeneration with at least two independent loss-of-function alleles and/or RNAi knockdown affecting the respective gene. In these experiments, the ''*SNCA* only'' genotype was compared with the ''Phenocopy'' genotypes as follows, in paraffin sections:

- ''*SNCA* only'': *Rh1-GAL4/+*; *UAS-SNCA.WT/+*
- ''Phenocopy - additional allele'': *Rh1-GAL4/+*; *UAS-SNCA.WT/additional allele*
- ''Phenocopy - RNAi'': *Rh1-GAL4/+*; *UAS-SNCA.WT/UAS-RNAi*

Generation of GlyRS *CRISPR-Cas9 alleles and corresponding genomic rescue transgene*

To generate CRISPR-Cas9 alleles in the *GlyRS* gene, we crossed *P{TKO.GS00715}attP40*, a transgenic strain expressing a guide RNA targeting the coding region, to *P{nos-Cas9.R}attP40*. The mutation was generated on a third chromosome of the isogenic *Iso7* background, which was used to generate EMS mutants in the modifier screen. This resulted in 27 lethal strains which failed to complement the $GlyRS^{08-107}$ from the chemical mutagenesis screen. Lethality of two of the CRISPR-Cas9 alleles, $GlyRS^{C2}$ and $GlyRS^{C27}$ could be rescued with a genomic transgene that includes a 4.15 kb genomic region containing *GlyRS* (nucleotide positions 15094265 to 15098415 of *D. melanogaster* genome r6.47).

Maintenance of Drosophila *alleles of* SNCA*-modifier genes*

We have found that their modifier phenotypes are susceptible to the accumulation of suppressors in the fly stocks. It has been necessary to outcross each modifier to a control genetic background prior to assays for phenotypes related to neurodegeneration.

Temporal control of RNAi expression in *SNCA*-expressing flies using the TARGET system

We used the *nSybQF2 QUAS-SNCA* transgenes to constitutively express *SNCA* in all neurons,[14,145] while using the *elav-GAL4 Tub-GAL80^{ts}* driver to conditionally express *skd/Med13* RNAi, *Pgi* RNAi or *EGFP* RNAi by keeping the flies at 18°C during early development and shifting them to 29°C in the adult stage. The TARGET system works through the ubiquitously expressed GAL80^{ts} which inhibit GAL4 activity at 18°C; at 29°C, GAL80^{ts} is no longer capable of inhibiting GAL4, hence allowing RNAi transgenes with *UAS* promoters to express.[146] The 18°C incubation during early development suppresses RNAi expression and avoids lethality or potential confounding effects on the developmental control of neuronal numbers.

Whole mount immunohistochemistry of fly brains

Drosophila larva and adult brains were dissected in PBS and fixed in 3.7% paraformaldehyde in PBS. The primary antibodies used were chicken anti-α-synuclein (Abcam, ab190376, 1:500), rabbit anti-Pgk2 (Merck, HPA073656, 1:500), rabbit anti-Pgi (Merck,

HPA024305, 1:500), rabbit anti-phospho histone H3 (PH3 Ser10, Millipore, 06–570, 1:500), rabbit anti-Tyrosine Hydroxylase (TH) (Pel Freeze, P40101-0, 1:300), mouse anti-PCNA (Thermo Fisher, PC10, 13–3900, 1:100), mouse anti-Elav (Developmental Studies Hybridoma Bank (DSHB) clone 9F8A9, 1:500 of concentrated antibody), rat anti-Elav (DSHB clone 7E8A10, 1:500 of concentrated antibody), anti-LDH (OAAB06120, Aviva Systems Biology, 1:500), rabbit anti-Sima/HIF (kind gift of Pablo Wappner, 1:500),[147] mouse anti-*Drosophila* Polo kinase (kind gift of David Glover, 1:500),[148,149] guinea pig anti-Deadpan (kind gift of Cai Yu, 1:500).[150]

For the counting of dopaminergic neurons in the protocerebral anterior medial (PAM) cluster and the optic lobe, brains co-labeled with anti-TH and 4′, 6-diamidino-2-phenylindole (DAPI) were analyzed with Imaris (Oxford Instruments) to identify and count nuclei that were surrounded by TH staining.

For immunohistochemistry of the retina, the brain was detached from the body, cut into two-halves in PBS and fixed in PBS with 0.1% Triton X-100 and 3.7% paraformaldehyde for 1 h at room temperature. Then lamina was dissected and cut along the length of ommatidium into 2–3 slices using a micro-scissor in PBS. The retina slice with the largest area and perfect cutting angle was selected and treated in PBS with 5% hydrogen peroxide and 0.4% Triton X-100 at 37°C for 4 h to make the slices colorless. Slices were further washed with PBS and permeabilized in PBS with 20% DMSO, 0.1% Tween 20, 0.1% Triton X-100, 0.1% Sodium Deoxycholate and 0.1% NP-40 at 37°C overnight, then washed with PBS with 0.4% Triton X-100 for immunostaining.

Imaging of genetically-encoded biosensors in fly neurons

Biosensors for glutathione (GSH) oxidation and hydrogen peroxide

For the imaging of GSH oxidation status and hydrogen peroxide, we used the genetically-encoded sensors cyto-Grx1-roGFP2 and mito-roGFP2-Orp1, respectively. The genetically-encoded sensor for glutathione, cyto-Grx-roGFP2, shows ratiometric changes in fluorescence in a manner that depends on the GSSG:GSH ratio.[151] On the other hand, mito-roGFP2-Orp1 undergoes ratiometric fluorescent changes in response to hydrogen peroxide.[152] Briefly, each fly brain was dissected and immediately transferred to PBS with 20 mM N-Ethylmaleimide (NEM, Thermo Fisher Scientific) and 3.7% paraformaldehyde at room temperature to fix for 1 h. Then brains were washed in PBS with 0.4% Triton X-100 and 5% Goat serum at 4°C overnight to reduce the effect of empty trachea on imaging. Brains were mounted in ProLong™ Gold Antifade Mountant (Thermo Fisher Scientific) and imaged on the same day. Images were processed and analyzed with Imaris (Oxford Instruments), with the 405/488 ratio defined as the intensity mean in channel 405 divided by intensity mean in channel 488.

Analysis of mitochondrial morphology

For the imaging of mitochondrial shapes and volumes using mito-roGFP2-Orp1 as the label, z-stacks of the lamina were acquired at 0.34 μm intervals on an FV3000 Olympus confocal microscope. Mitochondrial shapes and volumes were analyzed with Imaris (Oxford Instruments). To analyze mitochondrial shapes, the Ellipticity Prolate measurement was used because this measurement examines how long the longest axis is relative to its width. For example, a mitochondrion with a tube-like or cigar-like morphology will have Ellipticity Prolate closer to 1 than one that is more spherical.

Biosensor for ATP (AT1.03NL)

For the imaging of the ATP sensor, AT1.03NL, each brain was dissected in cold *Drosophila* Schneider's Medium (Thermo Fisher Scientific) and imaged on an FV3000 Olympus confocal microscope. By exciting AT1.03NL with the 405 nm laser, the CFP signals and the FRET signals were collected in the 465–495 nm and 525–600 nm ranges, respectively. Images were processed using Fiji/ImageJ by analyzing 8–14 stands of en passant synapses per fly, and the mean FRET/CFP ratio of all analyzed synapses from each fly is expressed as the ATP index of the fly.

Biosensor for ATP (in vivo luciferase assay in free moving flies)

Free-moving flies were fed the cell-permeant luciferin which was metabolized in an ATP-dependent manner to release photons, as described elsewhere.[77] Melted fly food (corn meal agar) was cooled to 45°C before luciferin (Gold Biotechnology LUCK-2G) was dissolved to a final concentration of 15 mM. The luciferin-containing food was dispensed into the wells of a black 96 well plate and allowed to cool (Sigma-Aldrich, BR781608-100EA). Flies immobilized on ice were then placed into individual wells. The plate was sealed with optical sealing film and tiny holes made above each well with a gauge 25 needle for gaseous exchange. The plate was then placed into a Tecan Spark Plate Reader for repeated measurements of bioluminescence from luciferase over 20 h. This method has the advantage of revealing ATP levels specifically in neurons due to the neuron-specific expression of transgenic luciferase.

Biosensor for lactate

For the imaging of the lactate sensor, Laconic, each brain was dissected in *Drosophila* Schneider's Medium (Thermo Fisher Scientific) and imaged on an FV3000 Olympus confocal microscope. By exciting Laconic with the 445 nm laser, the CFP signals and the FRET signals were collected in the 480–520 nm and 530–590 nm ranges, respectively. Images were processed using Fiji/ImageJ by analyzing the horizontal lobes of the mushroom body, and the mean FRET/CFP ratio from each fly is expressed as the FRET ratio of the fly. The mushroom body horizontal lobes were chosen because the PAM neurons, which are responsible for startle-induced locomotion, form synapses on the horizontal lobes of the mushroom body.

The experimenters were blinded to the genotypes of the samples to avoid bias.

Quantitative real-time PCR of fly transcripts

50 fly larva brains or adult brains were dissected in PBS and placed in RNAlater (Thermo Fisher Scientific, R0901-100ML). RNA was extracted using RNAzol RT (Sigma-Aldrich, R4533) and genomic DNA was removed using dsDNase (dsDNase, Thermo Fisher Scientific, EN0771). RNA concentration was measured using NanoDrop-2000 Spectrophotometers (Thermo Fisher Scientific) and equal amounts of RNA was used for cDNA synthesis using RevertAid First Strand cDNA Synthesis Kit (Thermo Fisher Scientific, K1621). qPCR was performed using Maxima SYBR Green/ROX qPCR Master Mix (2X) (Thermo Fisher Scientific, K0221) on a Fast Real-Time PCR System (Applied Biosystems, ABI7900HT). Primers targeting the transcripts of two genes, *Rpl32* and *ed*, are used as internal controls to normalize qPCR data. *Rpl32* and *ed* are considered as good internal controls because their respective transcripts levels did not change in response to neuronal *SNCA* expression in a previous RNAseq study.[153] The qPCR data was processed as previously described,[154] and *Rpl32* and *ed* levels were used jointly to normalize the levels of each transcript of interest. The primer sequences are listed in Table S3.

Western blot analysis of fly tissue lysates

Fly larva brains or adult brains were mechanically lysed in the following buffer: 10 mM Tris-HCl pH 8.0, 200 mM NaCl, 1% Triton X-100, 5 mM EDTA, 5% Glycerol, 1 mM Dithiothreitol, 0.5 mM PMSF and protease inhibitor cocktail (Sigma-Aldrich, 4693116001). Laemlli buffer was added to lysates to a final concentration of 1x (~1% SDS), and the mixture heated to denature the protein. The lysates were electrophoresed in 4–20% stain-free gradient gel (Bio-Rad, 4568096) and the stain-free total proteins were imaged in ChemiDoc MP (Bio-Rad) before transfer onto PVDF membranes. Tris-Glycine transfer buffer with 20% methanol was used. Modifications were made in the transfer protocol for the following proteins: (1) for Sima and Skd, 0.05% SDS was added to transfer buffer to facilitate the transfer of these large proteins, (2) α-syn, the PVDF membrane was fixed in PBS with 0.37% PFA for 0.5 h after transfer as described previously.[155] All the primary antibody dilution was 1:1000 except 1: 20,000 for alpha-tubulin. The primary antibodies used were anti-Skd (gift of Jessica Treissman, 1:1000), anti-Sima (Rb anti-Sima, gift of Pablo Wappner, 1:1000), anti-α-synuclein (Abcam, ab190376, 1:1000), anti-α-synuclein (clone 42, BD Biosciences, BD610787, 1:1000), anti-phospho-α-synuclein Serine 129 (clone D1R1R, Cell Signaling Technology, 23706),[156,157] anti-PGK (Merck, HPA073656, 1:1000), anti-PGI (Merck, HPA024305, 1:1000), anti-LDH (OAAB06120, Aviva Systems Biology, 1:1000) and anti-alpha-Tubulin (DSHB 12G10, 1:20000).[63,147] The images were acquired using ChemiDoc MP (Bio-Rad) and band intensity was analyzed using Image Lab (Bio-Rad), processed in Microsoft Excel, and plotted in GraphPad Prism.

For the Western blot of adult fly heads to analyze levels of total α-syn and pS129 phosphorylation, the sample preparation method is the same as above except for the inclusion of Phosphatase Inhibitor Cocktail 3 (Sigma-Aldrich P0044) in the lysis buffer.

Western blot analysis of mouse brain lysates

Western blotting was performed following a standard protocol. Proteins were extracted by cell lysis buffer (RIPA cell lysis buffer, PPLYGEN, C1053) and the protein concentration was determined by BCA Protein Assay Kit according to the manufacturer's instruction. Brain lysates (~20 μg of total protein) were boiled in 5 × SDS loading buffer for 10 min and loaded onto a 4–12% Criterion™ TGX Stain-Free™ Protein Gel (Bio-Rad Laboratories) before transferring to a polyvinylidene difluoride PVDF membrane (Bio-Rad Laboratories). Membranes were blocked with 5% slim milk. The membrane was then probed with corresponding primary antibodies at 4°C. The primary antibodies were: mouse anti-MED13/TRAP240 (Santa Cruz Biotechnology, sc-515557), mouse anti-beta actin (Abcam, ab8226), rabbit anti-PGK (Merck, HPA073656), rabbit anti-Pgi (Merck, HPA024305), rabbit anti-LDH (OAAB06120, Aviva Systems Biology), rabbit anti-MED12 (Abcam, ab70842), rabbit anti-CDK8 polyclonal antibody (Thermo Fisher Scientific, A302-501A-T), rabbit anti-Cyclin C polyclonal antibody (Thermo Fisher Scientific, A301-989A), rabbit anti-CRSP1/TRAP220 polyclonal antibody (Thermo Fisher Scientific, A300-793A) and rabbit anti-MED15 polyclonal antibody (Thermo Fisher Scientific, A302-422A). After washing, membranes were then incubated with appropriate horseradish peroxidase (HRP)-conjugated secondary antibodies. The immunoreactive bands were visualized using ECL Super Sensitive Kit (DE2002-500, DiNing) by ChemiDoc XRS+ System (Bio-Rad) and quantified by ImageJ.

Stereotaxic injection of adeno-associated virus (AAV) with short hairpin RNA (shRNA) and TH-positive cell counting

AAVs were purchased from HanBio (Shanghai). Two μl of *HBAAV2/9-EGFP NC* (1.3×10^{12} viral genomes/mL) or *HBAAV2/9-m-MED13 shRNA1-EGFP* (1.0×10^{12} viral genomes/mL) was infused unilaterally to the substantia nigra of five-month-old mice by stereotaxic injection at following coordinates (relative to the bregma): AP = 3.2 mm posterior; ML = 1.1 mm; DV = 4.2 mm at a rate of 0.4 μL/min 6 weeks later, mice were sacrificed and coronal sections of 25 μm thick were collected serially starting at 2.46 mm from bregma and ending at 4.04 mm from bregma. Sections were selected at intervals of 100 μm and processed for immunohistochemistry with chicken anti-tryosine hydoxylase (TH, Abcam ab76442). The shRNA sequences for *HBAAV2/9-EGFP NC* and *HBAAV2/9-m-MED13 shRNA1-EGFP* are indicated in Table S3.

The number of TH^+ neuron cells in the mouse substantia nigra (N) was calculated using design-based unbiased stereology described previously.[158] Briefly, the total number of TH^+ neuron cells in the substantia nigra is calculated with the following equation:

$$N = \Sigma Q \times t/h \times 1/asf \times 1/ssf,$$

where ΣQ is defined as the total number of TH^+ neuron cells counted in one brain section, *h* is height of the optical disector, *t* is the measured thickness of the section, *asf* is the area sampling fraction (the ratio of optical area in the whole grid) and *ssf* is the section sampling fraction (the ratio of section imaged in the total brain).

Immunohistochemistry of mouse brain

After each mouse is sacrificed, a 23-gauge butterfly needle was injected into the left ventricle of the heart and then PBS infused at a rate of 2 mL/min for 5 min, followed by perfusion of 4% paraformaldehyde solution at a rate of 2 mL/min for 5 min. Brains were removed and immersed in 4% paraformaldehyde solution at 4°C overnight. After dehydration in 20% sucrose, brains were embedded in O.C.T. compound (Sakura, 4583). Brain sections (10 μm) were prepared with a sliding microtome (Leica, Wetzlar, Germany). Brain slices were washed with PBS and treated with blocking solution (1% BSA, 0.4% Triton X-100 and 4% goat serum in PBS) for 1 h. Next, brain slices were incubated overnight at 4°C with primary antibodies diluted in blocking solution. The primary antibodies were: mouse anti-HIF-1 alpha (Abcam, ab1), mouse anti-MED13/TRAP240 (Santa Cruz Biotechnology, sc-515557), rabbit anti-PGK (Merck, HPA073656), rabbit anti-Pgi (Merck, HPA024305), rabbit anti-LDH (Aviva Systems Biology, OAAB06120), rabbit monoclonal [EPR15581-54] to TOM20 (Abcam, ab186735), Chicken polyclonal to Tyrosine Hydroxylase (Abcam, ab76442), rabbit monoclonal [EPR12763] to NeuN (Abcam, ab177487) and Rabbit monoclonal [MJFR1] to Alpha-synuclein (Abcam, ab138501). Brain slices were then washed with a washing buffer (0.1% Tween in PBS) and incubated with corresponding secondary antibodies diluted in PBS containing 0.3% of Triton X-100 for 3 h. After washing with PBS or washing buffer and PBS (when indicated), brain slices were embedded in Vectashield medium. Immunofluorescence images were captured at room temperature using a Zeiss confocal microscope using 20× or 40× objectives.

Analysis of mitochondrial aspect ratio in mouse brain slices

Mitochondrial morphology was visualized by immunostaining with anti-TOM20 antibody. The mitochondrial aspect ratio was quantified using a previously described Mitochondrial Network Analysis (MiNA) toolset on Fiji (ImageJ).[159,160] Briefly, the method processes two-dimensional images of mitochondria through a series of background subtraction, despeckling, local contrast enhancement and identification of mitochondrial network (Figure S7F).

QUANTIFICATION AND STATISTICAL ANALYSIS

Quantification of *Drosophila* climbing assay using the FlySpotter code

By careful optimization of the lighting of the climbing arena (METHOD DETAILS), flies were visible as dark objects on a brightly and uniformly lit background, and thus their positions could be easily detected using simple thresholding and filtering in the MATLAB-based FlySpotter code (Mathworks, Natick, MA). Positions of flies, corresponding to the heights they climbed up the cylinder, were then processed in Excel and plotted using GraphPad Prism. The climbing distance for each fly was pooled for each genotype for comparison. We have made the code we used for this analysis available at https://github.com/sg-s/fly-spotter.

Additional image analysis and quantification

Western blot images were analyzed using the Image Lab software (Bio-Rad). Immunofluorescent images were analyzed using FIJI (ImageJ) and/or Imaris (Oxford Instruments).

Statistical analyses

Statistical analyses were performed using Graphpad Prism (Dotmatics). The specific statistical test for each dataset is indicated in figure legend. The type of statistical test chosen for each dataset is dependent on the nature of the data.